IOP Publishing Journal of Physics: Condensed Matter
J. Phys.: Condens. Matter **32** (2020) 153002 (28pp) https://doi.org/10.1088/1361-648X/ab5e57

Topical Review

Thermal transport of carbon nanomaterials

Xue-Kun Chen[1,2] **and Ke-Qiu Chen**[1,3]

[1] Department of Applied Physics, School of Physics and Electronics, Hunan University, Changsha 410082, People's Republic of China
[2] School of Mathematics and Physics, University of South China, Hengyang 421001, People's Republic of China

E-mail: keqiuchen@hnu.edu.cn (K-Q Chen)

Received 21 December 2018, revised 17 October 2019
Accepted for publication 3 December 2019
Published 10 January 2020

Abstract

The diversity of thermal transport properties in carbon nanomaterials enables them to be used in different thermal fields such as heat dissipation, thermal management, and thermoelectric conversion. In the past two decades, much effort has been devoted to study the thermal conductivities of different carbon nanomaterials. In this review, different theoretical methods and experimental techniques for investigating thermal transport in nanosystems are first summarized. Then, the thermal transport properties of various pure carbon nanomaterials including 1D carbon nanotubes, 2D graphene, 3D carbon foam, are reviewed in details and the associated underlying physical mechanisms are presented. Meanwhile, we discuss several important influences on the thermal conductivities of carbon nanomaterials, including size, structural defects, chemisorption and strain. Moreover, we introduce different nanostructuring pathways to manipulate the thermal conductivities of carbon-based nanocomposites and focus on the wave nature of phonons for controlling thermal transport. At last, we briefly review the potential applications of carbon nanomaterials in the fields of thermal devices and thermoelectric conversion.

Keywords: thermal transport, carbon nanomaterials, phonon

(Some figures may appear in colour only in the online journal)

1. Introduction

Carbon, one of the most abundant elements in the Earth's crust, can exist in numerous allotropic forms, and these carbon allotropes are found to possess various functional properties, which make them very attractive subjects for both basic science and engineering applications. For instance, three-dimensional (3D) diamond is currently the hardest bulk material known, 3D graphite can serve as high temperature solid lubricants and 3D amorphous carbon materials are usually used as anode materials. In addition to these conventional bulk counterparts, a few low-dimensional carbon nanostructures such as 0D fullerenes, 1D carbon nanotubes and 2D graphene have been discovered and successfully synthesized in experiments [1–4]. Among them, graphene, a single layer of carbon atoms arranged in a honeycomb lattice, exhibits many interesting electronic properties due to its near-linear dispersive bands around the Dirac point, and holds great promise for enabling novel technologies for next-generation nanoelectronic devices [5–7]. In addition, graphene has an extremely high room-temperature thermal conductivity dominated by phonons [8–12], which is widely regarded as one of the most promising candidate for managing heat dissipation in integrated circuits by means of introducing graphene nanofiller to the polymer matrix. Similarly, carbon nanotubes (CNTs), described as rolled-up graphene sheets, are also promising for applications leveraging their unique electrical, thermal, and mechanical properties [13–17]. The encouraging performance of graphene and CNTs has also triggered considerable interest in exploring other low-dimensional carbon allotropes and

[3] Author to whom any correspondence should be addressed.

related isomorphic materials. For instance, graphyne and its family, another carbon network composed of hexagonal rings and acetylenic linkages, have attracted much attention because of their possible applications in spin filter devices [18–20], thermoelectric conversion element [21, 22], Li ion batteries [23], water desalination [24] and catalyst for dehydrogenation [25]. Recently, some new carbon allotropes like diamond nanothread [26], penta-graphene [27], pha-graphene [28] and carbon honeycomb [29] have been proposed with remarkable material properties that might outperform graphene. In short, the physicochemical properties of different carbon allotropes are closely related to the topological arrangement of carbon atoms and protrude the significance of structure-property relations.

Heat conduction in nanomaterials is one of the most fundamental issues in physics and technology. On the one hand, with the continuing miniaturization of characteristic dimension of integrated circuits (ICs), the dramatically increased power density inside ICs often leads to the formation of localized hotspots in electronic elements, which severely affects their reliability and performance. To effectively solve the thermal management issues above, it requires to increase the thermal conductivities of building materials used in the ICs, and to enhance the interfacial thermal conductance between fillers and matrix materials for electronic packaging. On the other hand, thermoelectric devices for waste heat recovery require materials with low thermal conductivity. Previous studies demonstrated that nanostructuring materials could obtain significantly higher thermoelectric efficiencies than those of bulk materials. First, the electron quantum confinement would result in the enhancement of Seebeck coefficient; and second, the additional phonon-boundary scatterings could reduce thermal conductivity of system [30–32]. In contrast to heat-conducting and thermoelectric conversion applications, the realization of functional thermal information devices like thermal diode [33], thermal transistor [34], thermal logical gate [35] and thermal memory [36] to manipulate heat signals demands that the thermal conductivities of materials could be reasonably regulated according to the specific needs. Considering the thermal conductivities of carbon nanomaterials span an extraordinary large range—over five orders of magnitude [37] and can be further tuned by introducing external stress field or inside structural defect, so the use of carbon nanomaterials to develop various thermal control devices is very promising. To achieve the goal, it first needs to build a series of method and theory to quantitatively predict the thermal conductivity of different nanosystems and to efficiently explain the fundamental mechanism behind nanoscale thermal transport. At a macroscopic level, the law of heat conduction (also known as Fourier's law) states that the heat flux passing through a system is proportional to the thermal gradient across it, and the proportion coefficient, namely thermal conductivity, is a size-independent constant for a specific material. However, as the size of material decreases to the nanoscale level, ballistic phonon transport plays a main role and Fourier's law gradually breaks down. For example, the length dependence of thermal conductivity in CNTs following $\kappa \sim L^{\alpha}$ was predicted by molecular dynamics simulations [38–40] and then observed experimentally [41], which is ascribed to super-diffusive phonon transport. Xu *et al* [42] found that the thermal conductivity in suspended single-layer graphene diverges logarithmically with system size ($\kappa \sim \log L$) because of the 2D nature of phonons in graphene. Furthermore, various anomalous heat transport behaviors such as thermal rectification (TR) [43–45], negative differential thermal resistance (NDTR) [46, 47] and thermophoresis [48, 49] have also been discovered in various carbon nanomaterials. These exotic behaviors, together with the invalidation of Fourier's law, have attracted worldwide interest and have led to heated discussions.

It is well known that thermal transport in carbon nanomaterials is usually dominated by phonons [37, 50]. The phonon transport in different low-dimensional carbon structures presents diverse novel phenomena rather than only one characteristic due to the presence of phonon confinement effect in objects with small dimensions. Up to now, there have been a series of reviews on phonon transport in CNTs [51], graphene [52–54] and graphene-based materials [55–57], which provides an overview of the existing studies and guidance to future works. In this review, we focus on phonons transport in tailored carbon nanomaterials that are probably used to produce various thermal management devices, and attempt to build a physical picture of how phonons transfer their energy in these nanostructures. In section 2, we briefly review different simulation methods on heat conduction, and describe experimental techniques for measuring thermal conductivity of nanostructures. In section 3, we show the theoretical and experimental results for the thermal transport properties of some pure carbon nanomaterials and explain the underlying mechanisms from both the viewpoints of the particle and wave nature of phonons. Meanwhile, the influences of structural defects, chemisorption and strain on phonon transport are also discussed. In section 4, we present the recent progress made towards understanding thermal transport in carbon-based nanocomposites such as graphene/boron nitride (BN) heterostructures, CNTs/Si interface and carbon-based nanofillers. In section 5, we summarize a few important potential applications of carbon nanomaterials in information carriers and thermoelectric conversion. In the final section, section 6, we give our conclusions and outlook.

2. Theoretical methods and experiments

2.1. Theoretical methods

In the last decade, multiple theoretical approaches have been developed to predict the thermal conductivities of low-dimensional nanosystems [58–61], mainly including molecular dynamics (MD) simulations, non-equilibrium Green function (NEGF) theory and the Boltzmann transport equation (BTE).

2.1.1. Non-equilibrium Green function. The NEGF method originates from the quantum field theory and was initially developed to handle electrical transport. So far, this mature approach has been extensively used to simulate nanoscale electronic devices [62–65]. By making a few careful substitutions, the NEGF method can be applied to phonon transport.

This change was first adopted to study dielectric nanowires [66, 67], and then was used to explore phonon transport in various nanostructures like graphene nanoribbons (GNRs) [68–70], graphyne nanoribbons [71], defected CNTs [72] and carbon chains [73]. In general, the system studied is conceived as consisting of three parts, namely, the left semi-infinite lead, the central scattering region and the right semi-infinite region. The Hamiltonians of entire system can be written as

$$H = \sum_{\alpha=L,C,R} H_\alpha + \left(u^{\mathrm{L}}\right) V^{\mathrm{LC}} u^{\mathrm{C}} + \left(u^{\mathrm{C}}\right) V^{\mathrm{CR}} u^{\mathrm{R}} + H_n \quad (1)$$

where u^α is a column vector consisting of all the atomic displacement in region α, $H_\alpha = \frac{1}{2}(\dot{u}_\alpha)^T \dot{u}_\alpha + \frac{1}{2}(u_\alpha)^T K_\alpha u_\alpha$ represents coupled harmonic oscillators. H_n is nonlinear part of the interaction, V^{LC} is the coupling matrix of the left lead to the central region and K_α is the force constant matrix calculated using empirical force field or the first principle method. When outside temperature is low, the lattice vibration could be approximated as harmonic issue. Under the harmonic approximation, the retarded surface Green's functions for the leads

$$g^{\mathrm{r}}_\alpha = \left[(\omega + \mathrm{i}\eta)^2 - K^\alpha\right]^{-1}. \quad (2)$$

Then, the retarded Green's function of central scattering region can be expressed as

$$G^{\mathrm{r}}_\alpha = \left[(\omega + \mathrm{i}\eta)^2 - K^c - \Sigma^{\mathrm{r}}_{\mathrm{L}} - \Sigma^{\mathrm{r}}_{\mathrm{R}}\right]^{-1} \quad (3)$$

here $\Sigma^r_{\mathrm{L/R}}$ is the retarded self-energies of the left/right lead. In terms of the so-called Caroli formula, the phonon transmission function can be calculated as

$$T(\omega) = \mathrm{Tr}\left(G^r \Gamma_{\mathrm{L}} G^a \Gamma_{\mathrm{R}}\right) \quad (4)$$

where $\Gamma_\alpha = \mathrm{i}\left(\Sigma^r_\alpha - \Sigma^a_\alpha\right)$ is the coupling function of the lead. In the ballistic thermal transport limit, the phonon thermal conductance is given by the Landauer formula

$$\kappa_{\mathrm{ph}} = \frac{1}{2\pi}\int_0^{\omega_{\max}} \hbar\omega T(\omega)\frac{\partial f(\omega, T)}{\partial T}\mathrm{d}\omega. \quad (5)$$

Here f is the Bose–Einstein distribution, $\omega_{\max}$ is the maximum phonon frequency. If the nonlinear effect at the central scattering region is further considered, the effective transmission function is computed by:

$$T(\omega) = \frac{1}{2}\mathrm{Tr}\left[G^r\left(\Gamma_{\mathrm{L}} + \frac{1}{2}\Gamma_n - S\right)G^a\Gamma_{\mathrm{R}}\right] + \frac{1}{2}\mathrm{Tr}\left[G^r\Gamma_{\mathrm{L}}G^a\left(\Gamma_{\mathrm{R}} + \frac{1}{2}\Gamma_n + S\right)\right] \quad (6)$$

here the nonlinear effect is reflected in the extra terms. A detailed description of the calculation procedure is referred to the review articles by Wang *et al* [74].

At present, the NEGF as a quantum approach is more likely employed for the ballistic phonon transport, especially in the case of low-temperature or small system that wave effects on the discrete atomic lattice should be considered. Theoretically, combining NEGF and first principle calculations enables the phonon–phonon and electron–phonon interactions to be contained in theoretical results, without needing to fit any parameters, which could be directly compared with experiment results. However, the process will need huge compute resources so that the complex computational task is hard to finish.

2.1.2. Boltzmann transport equation. To describe the phonon transport in dielectric crystals, phonons are normally observed as particles regardless of their wave properties. The phonon propagating from the left to the right lead is given by the linearized Boltzmann transport equation (BTE) [75]

$$\mathbf{v}_\lambda \nabla T \frac{\partial n_\lambda}{\partial T} = \left(\frac{\mathrm{d}n_\lambda}{\mathrm{d}t}\right)_{\mathrm{scat}} \quad (7)$$

where n_λ is phonon occupation number and $\mathbf{v}_\lambda$ is the group velocity of phonon mode λ. The major difficulty in solving the transport equation comes from the collision term. The simplest approach is the relaxation time approximation (RTA), in which one can compute the relaxation time of a phonon, assuming that the occupation number of other phonons is in equilibrium (n^0_λ), namely, the Bose–Einstein distribution. Under the approximation, the collision term can be written as

$$\left(\frac{\mathrm{d}n_\lambda}{\mathrm{d}t}\right)_{\mathrm{scat}} = \frac{n^0_\lambda - n_\lambda(t)}{\tau_\lambda} \quad (8)$$

where τ_λ is the total relaxation time that contains different phonon scattering processes such as Umklapp scattering ($\tau_{\lambda,\mathrm{U}}$), point defect scattering ($\tau_{\lambda,\mathrm{pd}}$), impurity scattering ($\tau_{\lambda,\mathrm{i}}$) and boundary scattering ($\tau_{\lambda,\mathrm{b}}$). Using Matthiessen's rule assuming that all kinds of scattering mechanisms are independent of each other, τ_λ is given by

$$\tau^{-1}_\lambda = \tau^{-1}_{\lambda,\mathrm{U}} + \tau^{-1}_{\lambda,\mathrm{pd}} + \tau^{-1}_{\lambda,\mathrm{i}} + \tau^{-1}_{\lambda,\mathrm{b}}. \quad (9)$$

Based on the above derivation, the resulting expression for κ can be computed as the sum over the contribution of all independent phonon modes

$$\kappa = \frac{1}{V}\sum_\lambda C_\lambda v_{\alpha\lambda} v_{\beta\lambda}\tau_\lambda \quad (10)$$

where $C_\lambda = \hbar\omega\partial n^0/\partial T$ is the mode specific heat. v_{λ_α} is the phonon group velocity for the mode λ in the α direction.

The equation (10) requires as inputs the phonon dispersion relation, which describes the phonon frequency ω_λ for different wavevectors $\mathbf{q}$. To obtain the phonon lifetimes τ_λ, most BTE calculations are limited to considering the low-order anharmonic perturbation, namely, three-phonon scattering processes, in which energy and momentum conservation determine the following selection rules:

$$\omega_{\lambda_1} \pm \omega_{\lambda_2} = \omega_{\lambda_3} \text{ and } \mathbf{q}_1 \pm \mathbf{q}_2 = \mathbf{q}_3 + \mathbf{G} \quad (11)$$

here $\mathbf{G}$ is the reciprocal lattice vector. For normal (N) process, $\mathbf{G} = 0$. For Umklapp (U) process, $\mathbf{G} \neq 0$. It is worth pointing out that although the RTA considers both N and U scattering, however, treats N scattering as purely resistive, so that it could not describe the thermal transport of certain carbon-based materials well [76–78]. For 2D carbon nanomaterials such as graphene or graphyne, an additional selection rule [77, 78] is applied to consider the reflection symmetry perpendicular to

their planar lattice structure. The lifetime τ_λ can be computed as [79, 80]

$$\frac{1}{\tau_{\lambda_1}(\mathbf{q}_1)} = \frac{\hbar\pi}{4N_{q_1}\omega_{\lambda_1}(\mathbf{q}_1)} \frac{\left|V_{\lambda_1\lambda_2\lambda_3}(\mathbf{q}_1,\mathbf{q}_2,\mathbf{q}_3)\right|}{\omega_{\lambda_2}(\mathbf{q}_2)\omega_{\lambda_3}(\mathbf{q}_3)} \delta_{\mathbf{G},\mathbf{q}_1\pm\mathbf{q}_2-\mathbf{q}_3} \left[\tfrac{1}{2}\left(1+n_{\lambda_2}(\mathbf{q}_2)+n_{\lambda_3}(\mathbf{q}_3)\right)\delta\left(\omega_{\lambda_1}(\mathbf{q}_1)-\omega_{\lambda_2}(\mathbf{q}_2)-\omega_{\lambda_3}(\mathbf{q}_3)\right) + \left(n_{\lambda_2}(\mathbf{q}_2)-n_{\lambda_3}(\mathbf{q}_3)\right)\delta\left(\omega_{\lambda_1}(\mathbf{q}_1)-\omega_{\lambda_2}(\mathbf{q}_2)+\omega_{\lambda_3}(\mathbf{q}_3)\right)\right] \tag{12}$$

here $V_{\lambda_1\lambda_2\lambda_3}(\mathbf{q}_1,\mathbf{q}_2,\mathbf{q}_3)$ describes the anharmonic component of the interatomic potential which requires knowledge of the cubic force constants. The colocations of the cubic force constants are carried out by taking finite differences of harmonic force constants from first principles simulations, which is an extremely challenging calculation. n is the equilibrium phonon populations, and obeys the Bose–Einstein statistics. Furthermore, exact expressions for other scattering processes are available only for the simple point-defect, boundary, and impurity. For example, Xie *et al* [81] calculated the contributions ratio from three acoustic branches (LA, TA and ZA) to the thermal conductivity of graphene and considered the influence of point defect scattering on phonon transport by

$$\tau_{\lambda,\mathrm{dp}}^{-1} = \begin{cases} 2.25x\Omega\dfrac{\omega^3}{v_\lambda^2} & \lambda = \mathrm{LA,TA} \\ 1.125x\Omega\dfrac{\omega^2}{\alpha} & \lambda = \mathrm{ZA} \end{cases} \tag{13}$$

where x is the density of vacancies and Ω is the primitive cell area. Meanwhile, the effect of phonon-boundary scattering on the three acoustic branches has also been studied [82]. It is worth noting that under the long wavelength approximation, Nika *et al* [83] obtained the empirical expression for Umklapp scattering in terms of the Grüneisen parameter.

$$\tau_{\lambda,\mathrm{U}}^{-1} = \frac{\gamma_\lambda^2 k_\mathrm{B} T\omega^2}{M v_\lambda \omega_{\mathrm{D},\lambda}} \tag{14}$$

where M is the mass of unit cell, v_λ is the average phonon velocity for a given branch, γ_λ is the Grüneisen parameter and $\omega_{\mathrm{D},\lambda}$ is the Debye frequency. The significant simplification of phonon scattering processes often results in some ambiguity in the exact predictions of the thermal conductivities of low-dimensional nanosystems. More importantly, the coupling effect of different phonon scattering mechanisms is ignored in the present BTE solution.

2.1.3. Molecular dynamics simulations. The molecular dynamics (MD) simulation as a powerful tool can handle complex atomic level structures based on Newton's equation of motion. The advantage of the MD approach is to only demand the structural parameters and suitable empirical force field as the input, with almost no assumptions that might be made in other theoretical models. Generally, there are two typical ways to calculate the thermal conductivities of carbon nanomaterials in MD simulations. One is the non-equilibrium MD (NEMD) method, known as the direct method. In this method, a temperature gradient is imposed across the simulation cell by applying two thermostats at different temperatures to the two sides of the sample, and then it will induce a heat flux in the simulation cell, which is more similar to real experiment measurement. After sufficient run-time, the simulated system reaches the nonequilibrium stationary state where the heat flux and temperature gradient are constant, so the thermal conductivity can be obtained from Fourier's law of heat conduction

$$\kappa = -\frac{J}{\nabla T} \tag{15}$$

where J is the heat flux and ∇T is the temperature gradient along the heat transport direction. The calculation of J is made according to the energy injected into/extracted from the heat source/sink, and ∇T is extracted from the linear fitting of the temperature profile.

Alternatively, the equilibrium MD (EMD) method based on the fluctuation-dissipation theory can be used to study the directional-dependent thermal conductivity of carbon nanomaterials via the Green–Kubo formalism as given by

$$\kappa_{\mu\nu} = \frac{1}{T^2 k_\mathrm{B}\Omega}\int_0^\tau \langle J_\mu(t) J_\nu(0)\rangle \mathrm{d}t \tag{16}$$

where Ω is the volume of the simulation domain, k_B is the Boltzmann constant, $J_\mu(t)$ is the heat flux in the direction μ, $\langle J_\mu(t) J_\nu(0)\rangle$ denotes the ensemble average of the heat current autocorrelation function (HCACF), τ is the truncation time and the integration scheme has been proposed by Schelling *et al* [84]. Note that the choice of τ should be large enough to make the HCACF achieve convergence. To reduce the fluctuation of the calculated thermal conductivity, one should repeat the EMD simulation with different initial condition of the velocity distribution. Moreover, to overcome the finite-size effect on the calculated κ, periodic boundary conditions (PBCs) are often adopted in EMD simulations [85–87].

The MD simulations, intrinsically containing different phonon scattering processes, are widely applied to study the thermal transport properties of carbon nanomaterials with different atomic configurations, such as size-dependent thermal conductivity in CNTs [38–40, 88], the defect [89, 90], strain [91], chemisorption [92], interface [93, 94] and substrate [95, 96] dependence of the thermal conductivity in graphene. However, when ambient temperature is lower than the Debye temperature of system, there is a large discrepancy between MD simulation and fully quantum approach in the prediction of thermal conductivity. Subsequently, different quantum correction models like quantum temperature [97] and quantum Langevin heat bath [98, 99] have been prospered to mitigate this limitation of classical mechanics.

It is worth pointing out that κ obtained from MD simulations represents an average over all phonon modes, obscuring the characteristics of single-phonon mode. For this, McGaughey *et al* [100, 101] and Ruan *et al* [102, 103] respectively put forward the spectral energy density (SED) technology based on EMD simulations and lattice dynamics calculations, to compute the mode-wise thermal conductivity under the framework of linearized BTE. According to the equation (10), there are three physical quantities strongly affecting phonon mode contributions to thermal conductivity, namely phonon heat capacity, group velocity and relaxation time. For the classical system, $C_\lambda = \frac{k_\mathrm{B}}{V}$ and the group velocity of phonon mode λ can be calculated using the central difference method

$v_{\alpha\lambda} = (\omega_{\lambda+\Delta\lambda} - \omega_{\lambda-\Delta\lambda})/2\Delta q_\alpha$ or Hellmann–Feynman theorem

$$v_{\alpha\lambda} = \frac{1}{2\omega_\lambda} e_\lambda^T \frac{\partial D_\lambda}{\partial q_\alpha} e_\lambda \tag{17}$$

here D_λ is dynamic matrix, q_α is the wave-vector compoent in α direction and e_λ is eigenvector. As described above, the third physical quantity that needs to be determined is the phonon relaxation time. In the case of perturbation, it can be extracted by evaluating the normal mode coordinates and the SED function $\Phi_{\boldsymbol{q},\nu}(\omega)$

$$\dot{q}_{\boldsymbol{q},\lambda}(t) = \sum_{\alpha}^{3} \sum_{b}^{n} \sum_{l}^{N_c} \sqrt{\frac{m_b}{N_c}} \dot{u}_\alpha^{l,b}(t) \left(e_{b,\alpha}^{\boldsymbol{q},\lambda}\right)^* \exp\left[\mathrm{i}\boldsymbol{q}\cdot\boldsymbol{r}_0^l\right] \tag{18}$$

$$\Phi_{\boldsymbol{q},\lambda}(\omega) = \left| \int_{-\infty}^{+\infty} \dot{q}_{\boldsymbol{q},\lambda}(t)\, \mathrm{e}^{\mathrm{i}2\pi\omega t} \mathrm{d}t \right|^2 \tag{19}$$

where $\dot{u}_\alpha^{l,b}(t)$ is the α component of velocity of atom b in the lth unit cell with equilibrium position $\boldsymbol{r}_0^l$ and $\left(e_{b,\alpha}^{\boldsymbol{q},\lambda}\right)^*$ denotes the complex conjugate of the component for atom b of the eigenvector. According to the anharmonic theory, the SED function in the framework of frequency domain can be written as a Lorentzian function centered at $\omega_{\boldsymbol{q},\lambda}^{\mathrm{A}}$

$$\Phi_{\boldsymbol{q},\lambda}(\omega) = \frac{C_{\boldsymbol{q},\lambda}}{\left(\omega - \omega_{\boldsymbol{q},\lambda}^{\mathrm{A}}\right)^2 + \Gamma_{\boldsymbol{q},\lambda}^2} \tag{20}$$

$$\tau_{\boldsymbol{q},\lambda} = \frac{1}{2\Gamma_{\boldsymbol{q},\lambda}} \tag{21}$$

where $C_{\boldsymbol{q},\lambda}$ is a fitting constant for a particular mode. The equation (20) is effective when the linewidth $\Gamma_{\boldsymbol{q},\lambda} \ll \omega_{\boldsymbol{q},\lambda}^{\mathrm{A}}$. $\omega_{\boldsymbol{q},\lambda}^{\mathrm{A}}$ is the anharmonic phonon frequency, incorporating the frequency shift due to anharmonicity. In the curve fitting processing, a peak-detection algorithm is usually adopted to detect the location of peak in a spectrum. To quickly obtain fitting results, an initial guess of each parameter could refer to the phonon frequencies $\omega_{\boldsymbol{q},\lambda}^0$ obtained from harmonic-lattice dynamics.

2.2. Experiments

The experimental measurement of thermal conductivity of low-dimensional nanomaterials helps clarify the nature of heat carriers and understand the interfacial heat transfer behavior in electronic component like field effect transistor. With the development of nanofabrication technologies, it is possible to fabricate various nanostructures and measure the temperature gradient across the sample under different external conditions, although still a challenging task. For now, there are several methods of measuring the thermal conductivity of low-dimensional nanomaterials, e.g. the Raman optothermal method [8], the thermal bridge method [104, 105], the 3ω method [106–108] and the scanning thermal microscope [109]. Among them, the confocal micro-Raman and thermal bridge methods are relatively mature for measuring thermal conductivity in carbon nanomaterials and the latter two approaches are mainly applicable to detect the thermal interfacial resistance, or thermal conductivity of bulk materials.

For instance, using the combination of laser heating of a nanotube and Raman observation of temperature profile method, Hsu *et al* [110] measured the relative contribution ratio of the intrinsic thermal resistance in CNTs and the boundary resistance between sample and substrate. Despite all this, the thermal conductivity of CNTs in this study has not been given because the value of optical power absorbed in the heating layer was not clear. Subsequently, Li *et al* [111] replaced laser heating with electrical self-heating of CNTs and combined the Raman shift method to extract the radial temperature profile independent of boundary resistance, and demonstrated the thermal conductivity of CNTs as high as 2400 W m^{-1} K^{-1}. Moreover, using non-contact Raman optothermal method, the pioneering experimental measurements by Balandin *et al* [8] showed that single-layer graphene may have a thermal conductivity ranging from 2000 to 5000 W m^{-1} K^{-1} at room temperature, even higher than that of diamond. Based on the same method, Chen *et al* [112] studied the isotope effect on thermal conductivity of graphene. The measured results show that the increase of ^{13}C isotope concentration results in the large reduction of the thermal conductivity from ~2800 W m^{-1} K^{-1} for 0.01% ^{13}C to ~1600 W m^{-1} K^{-1} for 50% ^{13}C. Using the electro-thermal bridge method, Xu *et al* [42] measured the thermal conductivity of suspended CVD single-layer graphene, and observed the logarithmic dependence of thermal conductivity on the sample length L ($\kappa \sim \log L$) for L ranging from 700 nm to 9 μm, according with earlier theoretical predictions [113, 114]. Lately, Bae *et al* [115] reported that thermal conductivity of GNRs with $L = 260$ nm is reduced from 230 to 80 W m^{-1} K^{-1} as the width of the sample decreases from 130 nm to 45 nm via electro-thermal bridge method, which is attributed to the enhancement of edge roughness scattering.

Although new technologies and equipment for measuring thermal transport in low-dimensional nanosystems have obtained substantial progress over the last few years, many problems about controlling heat flow and detecting temperature at nanoscale remain unsolved. For the commonly used confocal micro-Raman, there are two primary aspects strongly affecting the measurement uncertainty of thermal conductivity. One is the Raman peak shifts weakly with temperature changes [116]; the other is the accurate determination of thermal contact resistance, which contributes unavoidably to the total measured thermal resistance. The latter problem is also the main challenge for the thermal bridge method. Besides the above challenges, the existence of polymer residue and inconsistency of sample qualities also leads to different thermal conductivity measurements by different research groups [117]. In response to these questions, some review articles were conducted to better understand the experimental results for measuring thermal conductivity in low-dimensional nanosystems. Wang *et al* [118] summarized the progress of measurement methods, and Xu *et al* [53] outlined different experimental techniques and theoretical approaches for

phonon thermal transport and analyzed the respective challenging issues. Cahill *et al* [119] explored issues associated with thermal measurement science and thermal processing at the nanoscale.

3. Thermal transport in pure carbon nanostructures

3.1. 1D carbon nanomaterials

3.1.1. Nanowires. Recently, Fitzgibbons *et al* [26] reported the synthesis of a new 1D carbon nanomaterial—diamond nanothread (DNT). This DNT structure can be regarded as the hydrogenated (3, 0) CNT connected with the so-called Stone–Walls (SW) transformation defects. Based on the first-principles method, it is reported [120, 121] that there are 15 different stable DNT structures by considering all possible bonding geometries within a one-dimensional stack of six fold rings, and all of that can be divided into three types: achiral, stiff chiral, and soft chiral. The presence of the SW transformations in DNT will enrich its mechanical and thermal properties. Using the MD simulations, the mechanical properties of the above-mentioned 15 DNT structures have been investigated and the obtained results showed that their mechanical properties are strongly dependent on structure topology, ambient temperature [122]. Additionally, Wu *et al* [123] showed that the axial stiffness of DNTs (665–850 GPa) is of the same order as CNTs, and their strength could reach 4.1×10^7 N $\cdot$ mkg^{-1}, exceeding nanotubes and graphene. Recent works indicated that DNTs possess excellent interfacial load transfer capability for nanofiber applications owing to covalent bonding [124], and might be applied in effective reinforcements for nanocomposites [125].

Using the NEMD simulations, Zhan *et al* [126] found that comparing with (3, 0) CNT, the thermal conductivity of DNT is very low and behaves sensitive to the sample length. More intriguing is that the DNT with a given sample length exhibits a superlattice thermal transport characteristic: the thermal conductivity decreases firstly and then increases with increasing the number of poly-benzene rings, and the minimum thermal conductivity corresponds to the crossover point from coherent to incoherent phonon transport. Ertekin *et al* [127] reported that in glassy DNTs, some low-frequency modes exists well-defined longitudinal or twist-like polarization, partly offsetting the negative effect on phonon transport from structural disorder. In addition, the thermal conductivities of glassy DNTs could be reduced by a factor of about 5 through defect engineering. Wei *et al* [128] found that the thermal conductivity of DNT forests under strain loading presents anisotropic feature.

3.1.2. Nanotubes. In the past few decades, the thermal transport properties of CNTs have been studied in numerous papers and reviews, thus we will briefly review on this topic. At extremely low temperature ($T \approx 0$ K), only four acoustic modes including two transverse acoustic (TA) modes, one twisting (TW) mode and one longitudinal acoustic (LA) mode, contribute to the thermal conductance (G) of CNTs, which yields $G = 4G_0(T)$, namely the quantization of thermal

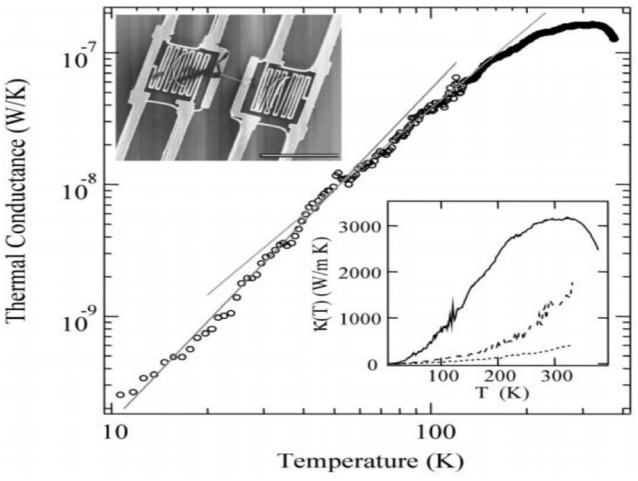

Figure 1. The thermal conductance of an individual MWCNT as a fucnction of temperature. The upper left inset represents a scanning electron microscopy (SEM) image of the suspended islands with the individual MWNT. The lower right inset denotes the thermal conductivity of an individual MWCNT with a diameter of 14 nm (solid line), 80 nm (dotted lines) and a large CNT bundles (dotted lines). Reprinted with permission from [131]. Copyright (2001) by American Physical Society.

conductance [129]. When T increases above a few degrees Kelvin, some low order optical modes are excited and participate in heat conduction that depends on the chirality and nanotube diameter. In this case, the phonon–phonon scattering could be negligible and the phonon-boundary scattering plays the dominant role in phonon transport. The obvious one is that thermal conductivity proportionally increases with T as the phonon modes increases and the phonon-boundary scattering rate remains constant [130], corresponding to the ballistic phonon transport. With further increase of temperature, the specific heat and thermal conductivity nonlinearly increase with T, and the function relation between them presents a faster than linear variation, which is called the intermediate transport regime. For instance, the measured thermal conductivity followed the $T^{2.01}$ trend as T increases from 50 K to 150 K in a multi-wall CNT (MWCNT) with 14 nm diameter based on heater sensor technique, while showed a $T^{2.5}$ dependence from 5 K to 50 K [131]. When temperature exceeds a certain critical value, the balance of increasing phonon population and strengthening phonon scattering is achieved, which corresponds to the maximum thermal conductivity. Regarding this respect, Fujii *et al* [132] found that the measured thermal conductivity of a MWCNT with a 16.1 nm outer diameter and a 4.9 nm inner diameter as a function of T reaches a peak (about 1700 W m^{-1} K^{-1}) at 320 K, which is broadly in line with theoretical prediction [133]. Kim *et al* [131] experimentally reported the thermal conductivity of MWCNT could approach 3000 W m^{-1} K^{-1} at 320 K and then decreased with temperature, as shown in figure 1. At higher temperatures, the system's thermal conductivity decreases with T due to Umklapp scattering processes, according with the characteristics of diffusive transport. For example, Maruyama *et al* [38] found that first-order Umklapp scattering gives rise to a T^{-1} dependence of thermal conductivity at high temperature. Pop *et al* [134]

observed that the thermal conductivity decreases more rapidly with T using self-heating technique, and attributed the subtle phenomenon to second-order three-phonon scattering with a scattering time proportional to T^{-2}.

Aside from temperature, length (L) is another key parameter to evaluate the ballistic transport or diffusive transport of phonons in nanotube. Tang *et al* [108] found an increase in thermal conductivity with L at 300 K via 3ω measuring technique, and estimated the mean free path of phonons to be around 180 nm. Using NEMD simulations, Maruyama *et al* [39, 40] found that the thermal conductivity of CNTs does not converge to a finite value even when the tube length reaches about 400 nm, but a power law relation ($\kappa \sim L^{\alpha}$) was observed, where α varies from 0.1 to 0.4, dependent on the chirality and temperature. The simulated results have also been confirmed experimentally [41]. Using BTE method, Mingo *et al* [130] showed that the thermal conductivity diverges as the nanotube length will increase if only three-phonon processes are considered during calculation, but inclusion of higher-order scattering processes will lead to the convergence of thermal conductivity. Using NEGF method, Yamamoto *et al* [135] found that the contribution of acoustic modes results in a power-law divergence $\kappa \sim L^{0.5}$ in CNTs. In general, for small L, the phonon transport is in ballistic regime and κ increase linearly with L; while L achieves several millimeters which is greater than the phonon mean free path, the phonon transport is dominated by diffusive conduction, so the thermal conductivity is insensitive to the change of tube length; For L falling within the intermediate range, the phonon transport transitions from the ballistic to diffusive regime with increasing L, and a power law $\kappa \sim L^{\alpha}$ might be fitted to the obtained results. Meanwhile, the tube-diameter dependence of the thermal conductivity of CNTs has also been explored, although some discrepancies exist between the results of different research groups. For instance, Yan *et al* [136] reported that the thermal conductivity of CNTs decreases with increasing the diameter (d) because the smaller the diameter of CNTs, the larger the phonon energy gap, and the lower the probability of phonon–phonon scattering. This is contrary to the argument of observation of Qiu *et al* [137] that the thermal conductivities of CNTs with different chirality increases with d. Lindsay *et al* [138] noted that there is a minimum in the thermal conductivity of CNTs as a function of d, which may be ascribed to the competition between the breaking of the graphene selection rule induced by nanotube curvature and the removal of phonon–phonon scattering conduction channels. Yue *et al* [139] found that an increase in d initially causes thermal conductivity to increase until it reaches a maximum value, and then it gradually decreases to the graphene limit. Besides the above three factors, there are some other factors such as vdW interaction [140, 141] and chemisorption [142] that can influence the thermal conductivities of CNTs.

As the analogues of CNTs, graphyne nanotubes (GNTs) also receive more attention due to their excellent electronic properties. To date, the thermal conductivity of GNTs has been studied in a few studies [143–145]. In particular, based on the NEMD simulations and SED analysis, Hu *et al* [143] investigated the thermal transport properties of GNTs, and found

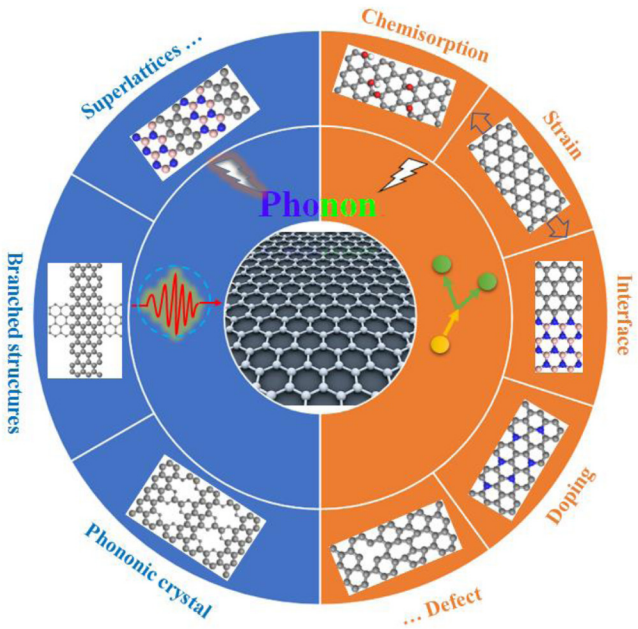

Figure 2. Schematic overview of various methods to control the thermal conductivity of graphene.

that the thermal conductivities of GNTs rapidly decrease with the increase of the number of acetylenic linkages (n). When $n = 10$, an unprecedentedly low thermal conductivity (below 10 W m^{-1} K^{-1}) was found in GNTs, which is attributable to the large vibrational mismatch between the weak acetylenic linkage and the strong hexagonal ring, causing inefficient heat transfer along the tube axis. Ramazani *et al* [144] believed that the significant decrease of the thermal conductivity in GNTs compared to that in CNTs has three causes: (1) lower acoustic group velocity, (2) shorter phonon relaxation times, and (3) smaller volumetric heat capacity. On the other hand, the naturally low thermal conductivity of GNTs is markedly advantageous for thermoelectric devices [146].

3.2. 2D carbon nanomaterials

3.2.1. Graphene and its derivatives. The ultra-high thermal conductivity of graphene has stimulated researchers' interest in exploring internal phonon transport mechanisms and potential applications for heat dissipation. Furthermore, the manipulation of the thermal conductivity of graphene may enable new applications of thermoelectric conversion and phonon devices. Actually, there have been some recent reviews on the thermal transport in graphene [52–54, 147–150]. For instance, AI Taleb *et al* [52] outlined recent progress made in the experimental determinations of phonon dispersion curves for graphene/metallic system, which could provide a detailed insight into the graphene-substrate interaction. Nika *et al* [54] provided a critical review of for phonon transport in graphene. In this review, they focused on the internal correlation between phonon spectrum and thermal conductivity in graphene-based nanomaterials, and discussed in detail the relative contributions of different phonon branches to the total thermal conductivity. Specially, a recently published book edited by Gang Zhang (2017) entitled 'Thermal transport in carbon-based

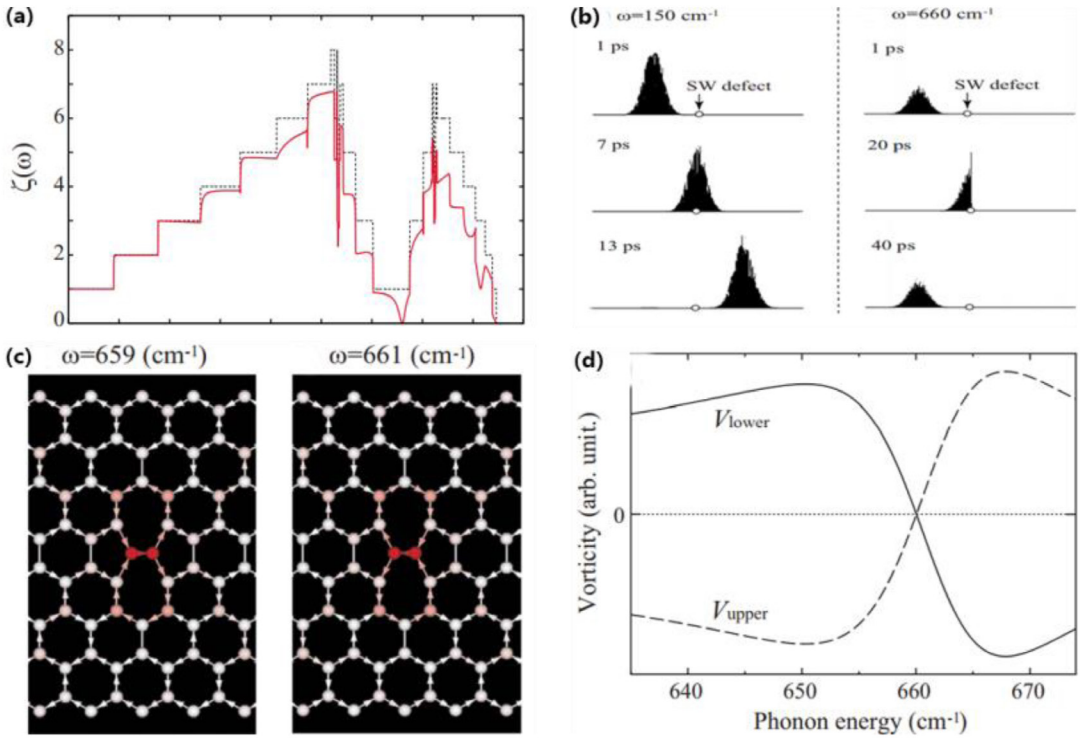

Figure 3. (a) The phonon transmission coefficient for out-of-plane phonons in ZGNR with SW defect (solid curve) and without defect (dashed curve). (b) Typical wave packet propagation process for two different phonon modes. (c) The phonon number and the bond thermal current around the SW defect for two phonon modes with $\omega = 659$ cm^{-1} and 661 cm^{-1} respectively. (d) The local vorticity with respect to the bond thermal current flowing on the upper dashed curve and lower solid curve heptagonal rings of the SW defect. Reprinted with permission from [170]. Copyright (2008) by American Physical Society.

nanomaterials' described the growth of graphene, its thermal property and applications in detail [151]. It is worth pointing out that these previous reviews mostly emphasize on the accuracy of the thermal conductivity value based on experimental measurement and theoretical simulation or the understanding of phonon characteristics in such 2D structure. Here, we highlight the manipulation of phonon transport in graphene.

Controlling nanoscale heat conduction is a complex task because of the quasi-particle nature (collective lattice vibrations) of phonons, wide range of phonon frequencies, and complicated atomic structures. For now, the most common route to control thermal conductivity is to enhance diffuse (particle-like) phonon scattering by introducing structural defects [152–154], vdW interaction [155–158], chemisorption [159, 160], and stress field [161–163]. In general, only a limited range of high-frequency phonons gets scattered efficiently, while low-frequency phonons with long wavelengths is hardly affected owing to their long mean free path. Recently, the phonon hydrodynamic transport have been predicted in graphene at higher temperatures and over a wide temperature range, which can be ascribed to strong N scattering processes and large density-of-states of long-wavelength ZA phonons induced by the 2D nature of graphene [164]. Moreover, in other 2D materials like boron nitride and graphane, it was found that the dominant scattering mechanism still works at all temperatures and heat transport in these 2D materials stratifies the conditions of Poiseuille and Ziman hydrodynamics, never reaching the ordinary conditions of diffusive transport even at very high temperatures [165]. Actually, similar results have been theoretically reported in 1D CNT [166] and 3D Graphite [167], which has been confirmed by recent experiment based on fast, transient thermal grating measurements [168]. In other word, between ballistic and diffusive transport, there is also a hydrodynamic transport that might provide a new picture to better understand heat conduction in graphene. Besides, a brand-new thought for manipulating thermal transport based on the wave nature of phonons such as phonon interference and phonon local resonance, is growing more and more appealing. A brief summary of various ways to control the thermal conductivity of graphene is shown in figure 2.

To be specific, Xie *et al* [169] studied the effect of single vacancy and Stone–Wales (SW) defects on the phonon transport of GNRs using the NEGF method. They found the single vacancy have a stronger effect on the thermal conductance of GNRs than SW defect, owing to the symmetrical breaking in GNRs with single vacancy. Analogously, Morooka *et al* [170] showed that there are two unique phonon transport phenomena in GNRs with SW defect: one is that the heat flux contributed by the lowest optical phonons mainly flows through the ribbon edges; the other is that the high-frequency phonons at $\omega \approx 660$ cm^{-1} is almost no contribution to the heat flux because of the formation of a circulating heat flux along the pairs of pentagon–heptagon rings in the SW defect, as shown in figure 3. The later was also confirmed by the phonon-wave-packet analysis technique. Moreover, Duan *et al* [171] presented the dependence of the thermal conductance on the extended line defects in GNRs that have observed in experiment [172], and found that the thermal conductance could be

tuned over wide ranges by changing the relative orientation between defect and transport direction. Using the Raman opto-thermal method, Chen *et al* [112] reported on an experimental study of isotope effect on the thermal properties of graphene, and observed the thermal conductivity from 2800 W m^{-1} K^{-1} for 0.01% isotope concentration to 1600 W m^{-1} K^{-1} for 50% isotope concentration at 380 K. Based on the same measuring method, Li *et al* [173] investigated thermal transport in twisted bilayer graphene and showed that the thermal conductivity of bilayer graphene is only half of that of single one. This can be understood that the emergence of numerous additional hybrid folded phonons in twisted bilayer graphene substantially enhances the phonon scattering. Morevoer, Malekpour *et al* [174] experimentally reported that as the defect density introduced by low-energy electron beam irradiation changes from 2×10^{10} cm^{-2} to 1.8×10^{11} cm^{-2}, the thermal conductivity of graphene decreases from 1800 W m^{-1} K^{-1} to 400 W m^{-1} K^{-1} near room temperature, which stems from the acoustic phonon-point defect scattering.

Strain engineering enables continuous tuning of the physical properties of materials, and is easily realized in experiment. For conventional bulk materials, compressive strain may cause the stiffening of phonon modes and enhance its thermal conductivity, whereas tensile strain usually softens phonon modes, resulting in reduced thermal conductivity. Wei *et al* [175] investigated different strain effects on the thermal transport in GNRs at room temperature. The simulated results demonstrated that the thermal conductivity of GNRs drops by 60% compared to the strain-free state as the tensile strain increases to 0.2, but is insensitive to the compressive strain. The analysis of phonon spectra indicated that under tensile loading, the strain-induced stress softens phonon modes and strengthens lattice anharmonicity; while under compressive loading, the open quasi-1D geometry of GNRs could form corrugations by which the stress from transverse deflection is released, and therefore the phonon modes is almost unchanged. Similar phenomena have been reported in previous studies [176–179]. Note that Yeo *et al* [178] found that the thermal conductance of GNRs with armchair edge (AGNRs) abnormally increase with the tensile strain at low temperature, while that of zigzag edge (ZGNRs) is hardly influenced by tensile loading. The reason of such variation was believed to be that the tensile strain slightly increases the out-of-plane acoustic modes in low-frequency range, which plays a decisive role in low-temperature phonon transport. Recently, Zhu *et al* [180] demonstrated a nonmonotonic dependence of the thermal conductivity of graphene on the tensile strain and this dependency was highly sensitive to the sample length. That is, for graphene with infinite length, its thermal conductivity increased to a peak value, after which it then decreases with further strain loading. The anomalous thermal conductivity variation was ascribed the competition between out-of-plane phonon stiffening favored in longer sample and in-plane phonon softening favored in shorter sample. Wang *et al* [181] studied the effect of the shear strain on the phonon transport in graphene, and found that the thermal conductivity of wrinkled graphene induced by shear strain can be reduced to 80% of the initial value, owing to the broadening phonon modes and increased low-frequency phonons.

Another effective approach to control the thermal conductivity of graphene or GNRs is chemisorption such as hydrogenated, oxidation and functionalization. Using NEMD simulations, Pei *et al* [182] investigated the thermal transport properties of hydrogenated graphene. The obtained results showed that for random hydrogenation, the thermal conductivity of such materials is reduced by more than 70% of the pristine value with increasing hydrogen coverage from 0% to 30%, and then becomes insensitive to further increasing coverage. The reason for reduced thermal conductivity could be probably due to the softening of the G-band phonon caused by the transition from sp^2 to sp^3 bonding upon hydrogenation. When the hydrogen distribution is patterned and parallel to the transport direction, the system's thermal conductivity monotonously decreases with increasing coverage from 0% to 100%. Barbarino *et al* [183] believed that the lower thermal conductivity in hydrogenated graphene with respect to the pristine one stems from the reduction of the acoustic phonon group velocity and the remarkable red-shift of high-frequency phonons. Luo *et al* [184] found that the thermal conductivity of graphene oxide with oxygen coverage of 5% is reduced by 90% compared to that of pristine one, and a coverage of 20% lowers it to 8.8 W m^{-1} K^{-1} even lower than the predicted amorphous limit for graphene. The analysis of phonon spectra revealed that two reasons were responsible for the dramatic decline in thermal conductivity: first, the presence of the oxygen atoms would introduce phonon-impurity scattering; second, the reflection symmetry of pristine graphene plane was broken in the region of oxygen coverage, to enhance phonon–phonon scattering involving flexural modes, as that in CNTs owing to the inherent curvature [76]. Chien *et al* [185] investigated the influences of methyl group and phenyl groups on the thermal conductivity of GNRs. It was found that a functionalization degree of 1.25% could reduce the system's thermal conductivity by nearly half, owing to the vibrational mismatch between sp^2 and sp^3 carbon atoms.

Given phonons are waves of the atomic lattice, so the wave interference of phonons might be used to manipulate heat flow as the remarkable success achieved when using photonic wave interference for manipulating light wave. Lately, a few papers were published on the manipulation of phonon transport in 1D nanowire and 3D phonon crystals based on the wave nature of phonons [186–188]. According to these studies, the necessary condition for interference effect is that the incident wave could retain their phases on reflection and transmission at interfaces. For this, high-quality superlattices as promising candidates could satisfied the above condition because of their atomically flat interfaces, in which some low-frequency phonons with long wavelengths are likely to occur specular reflection and forms wave interference; whereas high-frequency phonons are scattered diffusely. Then, the critical issue that should be addressed is to understand how the interference effect affects phonon transport process. On the one side, the presence of phonon wave interference will alter the phonon dispersion relations such as flattening branches of phonon dispersion

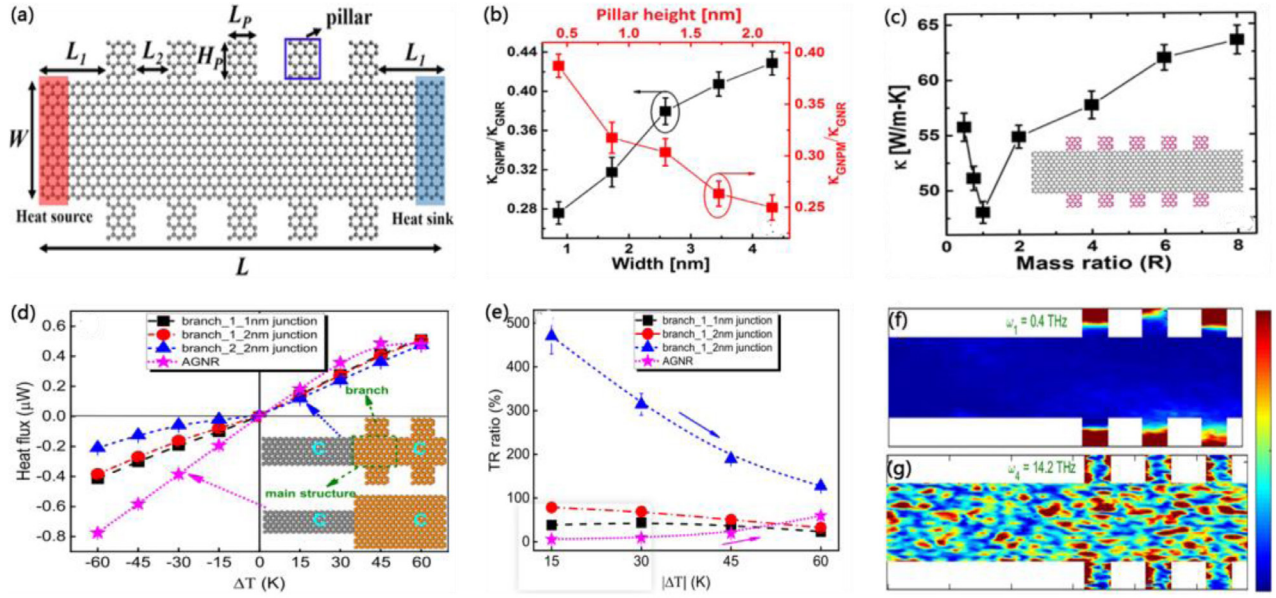

Figure 4. (a) Schematic picture of the branched GNR. (b) Thermal conductivity of branched GNR versus the width and pillar height. (c) Thermal conductivity of isotopic doped branched GNR with different mass ratio $R = M/12$, where M is the atomic mass of the isotope of carbon in the pillar. (d) Heat flux versus normalized temperature bias for pristine/branched GNR junctions. The insets are the configurations of the branched-2–2 nm junction and ZGNRs. (e) The TR ratio as a function of temperature bias. The spatial distribution of two phonon mode at (f) a resonant frequency (g) a nonresonant frequency, respectively. Reprinted figures (a)–(g) with permissions from [198, 199], respectively. The Copyright (2018) by American Physical Society and copyright (2018) by AIP Publishing LLC.

in a wider frequency range. For another, the interference effect may cause forbidden energy gaps in phonon spectrum. Luckyanova *et al* [189] experimentally observed that the measured thermal conductivity is linearly proportional to the total superlattice thickness at the low temperature range from 30 K to 150 K, and confirmed that the wave nature of phonons plays an important role in heat conduction. Ravichandran *et al* [190] measured the thermal conductivities of oxide superlattices with a fixed length as a function of the period length, and found that there is a local minimum value for the thermal conductivity. This is because for a large period length, most phonons are scattered diffusely at the interfaces and behave particle-like, while for smaller period length, a considerable portion of heat is carried by wave-like phonons experiencing interference effects. To control the phonon transport of graphene by wave interference effects, Luo *et al* [191] constructed $^{12}C/^{13}C$ graphene superlattices and calculated their thermal conductivities by NEMD simulations. The results demonstrated that the thermal conductivity in the superlattice with a period length of 0.8 nm increases linearly with the sample length over large distances, showing completely the wave interference of phonons as well as the occurrence of brillouin zone folding. A similar phenomenon was found in isotope CNT superlattices [192]. Ouyang *et al* [193] studied the thermal transport properties of isotopic-superlattice GNRs using NEGF method, and found the thermal conductance of such superlattice strongly depends on the period length and the isotopic mass, which offers an available way for modulating the thermal conductance of GNRs. Meanwhile, Yang *et al* [194] designed a structure of graphene phononic crystal (GPC) and investigated the thermal transport property of GPC. The obtained results showed that the system's thermal conductivity is significantly reduced as compared with pristine graphene, and can be further tuned by increasing porosity and decreasing period length. Moreover, they also noted that the existence of porosity may lead to phonon localizations.

Lately, Hussein *et al* [195] found that the introduction of nanopillars in silicon thin films causes an increase in the number of heat carriers, but greatly reduces the thermal conductivity of such films. This is because that the pillars exhibit numerous local resonances that could hybridize with the propagating modes of thin films across the entire spectrum (namely the concept of phonon local resonance), which reduces the group velocities. Volz *et al* [196] reported that in branched alloy nanowires (an array of nanopillars is built on top of a free-standing nanowires), the low-frequency phonons could be easily manipulated by branch configurations like branch size and shape, and the high-frequency phonons have been effectively scattered by the atomic mismatch in alloy structures. Combining the effects of phonon local resonant and phonon scattering, an extremely low thermal conductivity of 0.9 W m^{-1} K^{-1} in branched alloy nanowires has been obtained. Besides, the resonant mechanism still plays a major role in phonon transport even if there is structural defect in branched nanowires, so it has obvious advantage over phonon wave interference. More importantly, the addition of branches is not expected to not scatter electrons, benefitting for thermoelectric applications, which is not equipped by the phonon scattering mechanism. Subsequent study also gave similar results for branched CNTs [197]. More recently, Ma *et al* [198] found that the thermal conductivity of branched GNRs is less than half of pristine ones, and further doping in branches could even enhance the thermal conductivity of such branched structures, as shown in figures 4(a)–(c). This

trend seems to be against common sense that isotopic engineering generally reduces the system's thermal conductivity. Phonon mode analysis and NEGF calculation revealed that replacing C^{12} to heavier (lighter) isotopic in branches would lead to the mismatch between the resonant modes contributed by branches and propagating modes across the ribbons, which weakens the hybridization level of the two kinds of modes and facilitates phonon transport. In the view of this, Chen *et al* [199] designed an efficient thermal diode based on pristine/branched GNR junctions, and found that the TR ratio in such junctions exceeds 400% under small temperature bias ($\Delta T = 30$ K), showing distinct superiority over other thermal diodes. The mechanism behind this phenomenon could be attributed to the local resonance of longitudinal phonons in branched GNR region under negative temperature bias, as shown figures 4(d)–(g).

3.2.2. Graphyne family. Graphyne (GY) can be built by replacing a certain proportion of carbon–carbon double bonds in graphene with the acetylenic linkages. Considering the different distribution and proportions of the acetylenic linkages, there are multiple types of GY, namely α, β, γ, δ, (6, 6, 12), (14, 14, 14)-GY and so on. Among them, a thin film of GDY has been successfully fabricated so far [200]. In the last decade, studies on the electronic, mechanical and thermal properties of graphyne family took off rapidly. Using the NEGF method, Ouyang *et al* [201] investigated the thermal transport properties of γ-GY nanoribbons, and the obtained results showed that the thermal conductance of such nanoribbons is only 40% that of GNRs and is insensitive to the acetylenic linkages. Chen *et al* [202] calculated the thermal conductivity of γ-GY as a function of the number of acetylenic linkages based on EMD simulations, and found that the lowest thermal conductivity in GY is 93% lower than that of graphene with a similar size at room temperature. However, when $T < 30$ K, the thermal conductance of GY exceeds that of graphene, which is almost independent of the nanoribbon width. The reason for this anomalous thermal behavior was believed to be that some coherent low-frequency phonons are excited under low temperature and has a significant contribution to thermal conductance. Besides the temperature factor, Zhang *et al* [203] studied the thermal conductivities of GY with different configurations including α, β, γ, and (6, 6, 12) ones via NEMD simulations. The analysis indicated that the presence of the acetylenic linkages results in low atom density, weak single bonds and lower thermal conductivity in GY. Moreover, they also found that the thermal conductivity of (6, 6, 12)-GY exhibited obvious directional anisotropy, distinguishing from other three types. Based on the previous findings, Wang *et al* [204] designed GY heterojunctions (GYHJs) made of two different GY, and showed that the GYHJs exhibit tunable thermal transport properties by changing the composition and type of GY. They also demonstrated that with the decreasing proportion of γ-GY, the thermal conductivities of GYHJs decrease linearly in the armchair direction; whereas for the zigzag direction, it first decreases, then tends to keep a constant value, and later increases, indicating significant anisotropy. Hu *et al* [205] calculated the thermal conductivity of seven type GYs with different configurations, and found that the thermal conductivity of (14, 14, 14)-GY behaves unexpectedly significant anisotropy. That is, the thermal conductivity along zigzag direction is two or three times larger than that along armchair direction. Lattice dynamics calculations revealed that this anisotropy stems from the lower contribution of high-frequency and short-wavelength phonons to total thermal conductivity in armchair (14,14,14)-GY. To meet different application requirements, the regulation of the thermal conductivity of GY is necessary. Zhou *et al* [206] demonstrated that the thermal conductance of defective β-GY is about five times smaller than that of perfect one because of the intensive localization of phonons induced by the phonon-defect scattering, benefitting the thermoelectric applications. Zhang *et al* [207] studied the influence of the oxygen adsorption on the thermal transport in γ-GY based on reactive force field, and showed that the system's thermal conductivity can be effectively modulated by altering the oxygen coverage. On the other side, when the applied tensile strain is smaller than 0.04, the tensile stress induced by strain loading exerts positive effect on thermal transport, thereafter, the thermal conductivity of GY decreases with further increasing the tensile strain.

3.2.3. Other 2D architectures. Except the above 2D planar carbon architectures, there is various buckled carbon allotropes. Among them, penta-graphene is the most typical representative, and the new format of carbon structure has been predicted to be not only dynamically and mechanically stable, but also to sustain high temperature up to 1000 K [27]. In experiment, the growth of oriented large-area pentagonal single-crystal graphene domains on Cu foils by CVD method means a significant step forward the fabrication of penta-graphene [208]. Based on the MD simulations, Cranford *et al* [209] observed a structural transition from penta-graphene to graphene under the conditions of temperature change and external strain. In addition, a few works have been conducted to investigate the thermal transport in penta-graphene. For instance, Using BTE method combined with first-principles calculations, Wang *et al* [210] predicted the intrinsic thermal conductivity of penta-graphene being about 645 W m^{-1} K^{-1} at room temperature based on the assumed thickness of 0.12 nm. With respect to graphene, the lower thermal conductivity of penta-graphene was attributed to the strong anharmonic effect induced by the vibrational mismatch of hybridized sp^2 and sp^3 bonding. Moreover, they also found a layer-independent thermal conductivity for the stacked penta-graphene, because this buckled structure breaks the selection rule of three-phonon scattering for 2D planar material [211]. It is well known that the estimated thermal conductivity from MD simulations strongly depends on the interatomic potentials being adopted, and different empirical potentials have their own accuracy in describing the specific properties of nanomaterials. For carbon nanosystems, there are multiple types of empirical potentials available, such as AIREBO potential, Tersoff potential, ReaxFF and EDIP potentials [212]. Winczewski *et al* [213] systematically tested 14 different empirical potentials available for elemental carbon with the scope to choose the potential

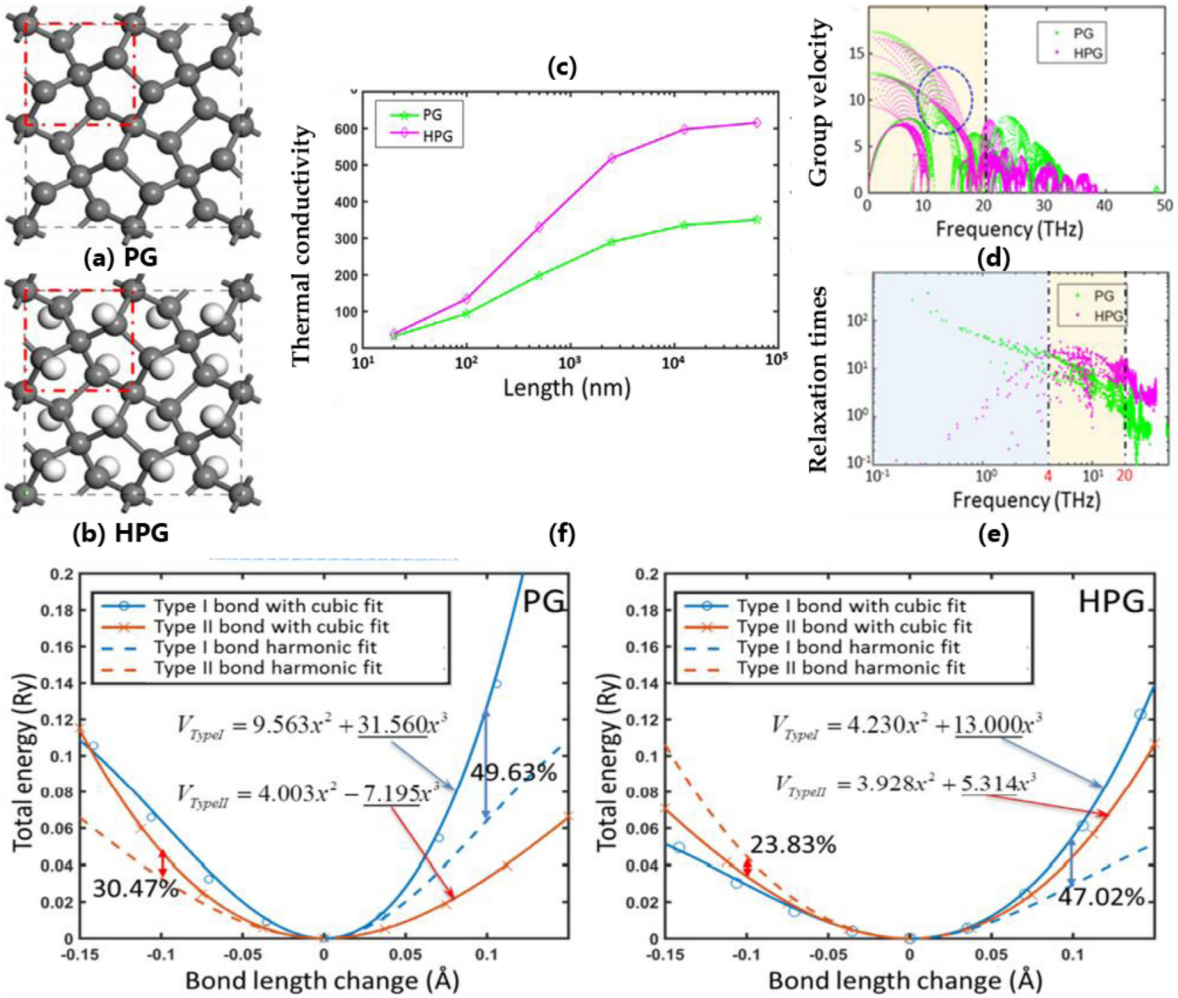

Figure 5. Atomic structures of (a) penta-graphene (PG) and (b) hydrogenated penta-graphene (HPG). (c) The thermal conductivity as a function of sample length for PG and HPG. (d) Phonon group velocities and (e) phonon relaxation times as a function of frequency for the two structures. (f) Bond energy as a function of bond length modulation for PG and HPG. Note that the absolute value of the nonlinear third-order coefficient indicates the relative bond anharmonicity. Reprinted with the permission from [216]. Copyright (2016) by American Chemical Society.

suitable for the modeling of penta-graphene. By comparing the obtained results with the principles calculations, they concluded that only the Tersoff potential proposed by Erhart and Albe in 2005 [214] is able to correctly describe all the important features of penta-graphene. Using EMD method with the original Tersoff potential, Li *et al* [215] calculated the thermal conductivity of penta-graphene at room temperature, and the obtained value was about 167 W m^{-1} K^{-1}, much lower than that of graphene. By performing SED analysis, they thought that there are two main causes for the lower thermal conductivity in penta-graphene: the lower phonon group velocities and fewer collective phonon excitations. As shown in figure 5, Wu *et al* [216] observed that the hydrogenation exerts positive effect on the thermal transport in penta-graphene (up to 76% increase), in contrast to hydrogenation of graphene which results in a dramatic decrease in thermal conductivity. The underlying mechanism for the abnormal increase of thermal conductivity was believed to be the weaker phonon–phonon scattering caused by the reduced bond anharmonicity in the hydrogenated penta-graphene. Zhang *et al* [217] revealed that the thermal conductivity of penta-graphene can be modulated by chemical functionalization. When the coverage was less than 25%, the system's thermal conductivity decreased rapidly with increasing coverage. Thereafter, the further increase of coverage would cause the enhancement in thermal conductivity.

3.3. 3D carbon nanomaterials

It is well known that graphene possesses many fascinating properties. However, it is difficult to retain such properties when integrating the 2D material into 3D nanodevices. Although multilayer graphene may be fabricated more easily, the presence of Vdw interactions between overlapping layers would degrade their performance on carrier mobility, tensile strength and heat dissipation. To overcome the drawbacks, it is desirable to build 3D graphene networks by the covalently bonded GNR segments. Some porous carbon nanostructures like Mackay–Terrones crystals [218] quadrilateral graphene network [219], carbon foam [220], pillared-graphene architectures [221, 222] and 3D CNT networks [157, 223] have been proposed theoretically and been demonstrated

to be dynamically stable, though their experimental synthesis might need further investigation. Lately, a new exceptionally stable 3D graphene, carbon honeycomb, has been successfully synthesized by deposition of vacuum-sublimated graphite and demonstrated high absorption level [29]. Furthermore, first-principles calculations and MD simulations showed that the carbon honeycombs have appealing specific strength [224], efficient anodes of Li batteries [225], tunable band gap [226] and Weyl semimetals [219] owing to the covalent nature of carbon–carbon bonds. In other words, the 3D networks inherit some excellent properties of graphene, and also offer other novel properties distinct from graphene. For thermal property, several research groups made efforts to evaluate the thermal conductivity of carbon honeycomb. For example, using EMD simulations, Wei *et al* [227] demonstrated that the thermal conductivity of carbon honeycomb along the honeycomb axis is comparable to the supported graphene (much better than most metal), and is about five times higher than that normal to the axis. The anisotropic thermal conductivity was explained by the direction-dependent elastic constants. Moreover, the effect of hexagon size and pressure on the thermal conductivity has also been explored in their work. Analogously, Chen *et al* [228] observed the anisotropic thermal conductivity in carbon honeycomb, and attributed it to the orientation-dependent phonon group velocities. Meanwhile, they also found the thermal conductivity has an inverse relationship with temperature, which results from the decreasing of the relaxation times (rather than specific heat or group velocity) of low-frequency phonons with increasing temperature via lattice dynamics analysis. In addition, Gu *et al* [229] showed that the effect of the chirality of the composed GNRs on the thermal conductivity of carbon honeycomb is nearly negligible, because the edges in different GNRs for honeycomb structure are similar. Using first-principle MD method, Han *et al* [230] thought that reconstruction of equidistant carbon atoms along the connection junctions makes the previously proposed model in experiment more thermodynamically stable. Based on the optimized model, they found an anomalous non-monotonic response of strain-engineered thermal conductivity for the 3D carbon network, in which the value of thermal conductivity reaches the maximum under a hydrostatic strain of 3%. The detailed analysis of phonon spectra revealed that the anomalous increase in thermal conductivity was attributed to the apparent improvement of phonon lifetime, which overwhelms reduced phonon group velocities caused by tensile strain. Zhang *et al* [231] constructed random carbon honeycomb structures with different degrees of cell irregularity by the Voronoi tessellation technique, and calculated their thermal conductivities via NEMD simulations. The calculated results showed that the system's thermal conductivity sharply reduces as the degree of cell irregularity increases.

4. Thermal transport in carbon-based nanocomposites

4.1. CNTs/bulk materials interface

For many applications including electronics packaging, vertically aligned CNT arrays with highly resilient mechanical properties are promising as thermal interface materials (TIM) to enhance the heat dissipation for nanoscale devices. To accelerate the practical application of CNTs as TIMs, most efforts have been devoted to improve the thermal interface conductance between CNTs arrays and the growth substrate or any films deposited on the top surface of the array. Normally, the contact resistance between CNT arrays and growth substrates is quite low because of the covalently bonded interface. Yang *et al* [232] and Wang *et al* [233] showed the thermal resistance of the vertical CNT/Si interface is to be in the range of 0.022–0.03 $Km^2 W^{-1}$. For the weak adhesion on the growth-opposite side of CNTs, the interfacial thermal resistance tends to be significantly larger because of unbonded interfaces. Son *et al* [234] observed that a thermal resistance of about 50 $Kmm^2 W^{-1}$ for multiwalled CNTs/SiO_2 interface, which is almost as the thermal resistance at some solid–solid interfaces, diminishing the advantage of CNT array as a TIM. Hence, several methods such as thermocompression [235] technique have been used to bond CNT arrays to substrates, enabling reducing the thermal interface conductance. Moreover, the effect of contacting surfaces and the roughness of the array on the thermal transport across the interfaces of CNTs and substrate have also been studied. Panzer *et al* [236] found that the variations in CNT heights give rise to the apparent thermal resistance because only small amounts of CNTs can completely contact both the top metal and the bottom substrate. Using NEMD simulations, Feng *et al* [237] studied the dependence of the interfacial thermal transport on the arrangement of CNTs, filling fraction, CNT diameter, environment temperature, and Vdw strength, and demonstrated that appropriate filling fraction (the arrangement of CNT) could enhance the interface thermal conductance by 91% (84%). Furthermore, the pressure loading in the vertical face of the CNT array can reduce the thermal resistance because of increasing the fraction of CNTs contributing to heat conduction. Except for CNTs vertically adsorbed on a substrate, there is a horizontal configuration of such nanotubes attached to the substrate, which is more relevant to heat dissipation using CNTs interconnects [238]. Furthermore, Ong *et al* [239] presented a simple expression for the thermal conductance (g) of CNTs/SiO_2 interface, which can be written as $g = 0.05D\chi(T/200)^{1/3}$. Here D is nanotube diameter, χ denotes the coupling strength between CNTs and SiO_2 and T is the ambient temperature. Kaur *et al* [240] experimentally showed that the higher the level of COOH-functionalization is, the more efficient the thermal exchange at the CNT-matrix interface is.

4.2. Graphene/other 2D materials interface

4.2.1. In-plane hybrids. It is well known that graphene possesses many outstanding physical properties. However, pristine graphene is a zero-band gap semiconductor, which makes it not suitable for electronics and optoelectronics applications. On the other side, beyond graphene, some other 2D materials such as hexagonal boron nitride (h-BN), silicene, molybdenum disulfide and phosphorene have been proposed and synthesized in recent years. Note that most of them have

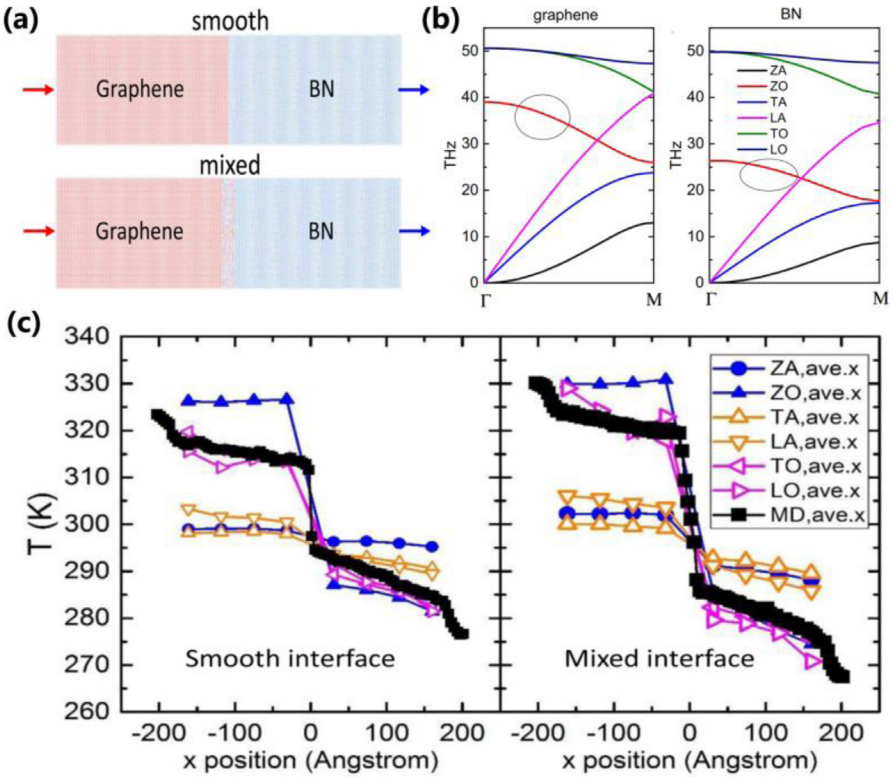

Figure 6. (a) The schematic model of graphene/BN interfaces. (b) The phonon dispersion relations of graphene and h-BN. Note that the ZO branches have negligible frequency overlap. (c) The T_{MD} with comparison to the spatial branch temperature of the phonons. Reprinted with the permission from [245]. Copyright (2017) by American Physical Society.

intriguing electronic characteristic like adequate energy band gap suitable for photosensing applications, meanwhile possess low thermal conductivity, which might give rise to problems in heat dissipation and operating power. To fully combine the advantages of graphene and other 2D materials, various graphene-based heterostructures are becoming a new focus because of their new physics and better device performance. Compared to the formation of vertically-stacked heterostructures by mechanical stacking, 2D in-plane heterostructures, with two materials linked by covalent bonds, may be more easily prepared benefiting from the advances in micro-technology. For instance, the development of the CVD method has shown the possibility to synthesize large-area 2D in-plane heterostructures with atomically sharp interfaces. It was reported that the graphene/h-BN in-plane heterostructures have been successfully fabricated using the CVD method [241]. Moreover, phosphorene/graphene in-plane heterostructure has also been synthesized by mechanochemical reaction [242]. In order to exploit graphene-based in-plane heterostructures for practical applications, it is necessary to investigate the thermal conductance across the heterostructure interfaces, and determine the role that graphene with ultra-high thermal conductive plays in solving the 'hot spots' issue.

Based on EMD simulations, researchers [243] calculated the thermal conductivity of hybrid graphene/h-BN heterostructures and found that the thermal transport perpendicular to the interface is insensitive to the BN concentration because of the dominant interface scattering and the less conductive component (BN) in the path of the heat flux. For the parallel transport, the thermal conductivity of the hybrid nanostructure attained a value close to the average of the two components, and monotonically decreases as the BN composition increases. From the view of phonon spectra, reduced thermal conductivity in the hybrid nanostructure was also thought to be that the participation ratios of phonons in the intermediate-frequency region decrease with increasing the BN concentration [179]. In other word, these phonons tend to be localized and the flow of heat flux have been partially blocked. Using the extended NEGF method, Ong *et al* [244] systematically studied the effect of strain and structure engineering on the thermal conductance at graphene/h-BN interface. They found that the applied tensile strain dramatically results in the enhancement of thermal conductance owing to the improved alignment of the flexural acoustic (ZA) phonon bands. More importantly, they also observed a unique phenomenon that the orientation of the transmitted optical phonons is strongly dependent on the interfacial configuration. To resolve phonon mode coupling across interfaces. Feng *et al* [245] developed a spectral phonon temperature technology that can extract the temperature of different phonon modes in both real and phase spaces within the framework of NEMD simulations. As shown in figure 6, for the benchmark material of graphene/h-BN in-plane heterostructure, strong coupling occurred between the acoustic phonon modes on both sides, and the contribution of out-of-plane optical (ZO) modes to the interface temperature drop is very large owing to the negligible phonon band

overlap between graphene and h-BN. That is, the phonon local thermal nonequilibrium provides a new perspective to understand the mechanism of thermal interfacial resistance.

During the growth process of graphene-based heterostructures, several defects such as single-vacancy (SV), and SW are unavoidably introduced into the interface [246]. Using NEMD method, Liu *et al* [247] showed that the presence of SW defects can enhance the interfacial thermal conductance because of lowered mismatch strain caused by misfit dislocations and the out-of-plane deformations screen. Li *et al* [248] systematically studied the effects of system dimension, environment temperature, SV and SW defects on the interfacial thermal conductance between graphene and h-BN, and showed that it decreases linearly with increasing SV concentration but slowly varies with small SW concentration, and then reaches a platform at a large concentration. In addition, the thermal transport in graphene/phosphorene and graphene/MoS_2 in-plane heterostructures has been studied by Zhang *et al* [249, 250]. The obtained results indicated that when the tensile strain is applied to the sample, the interfacial thermal conductance of armchair heterojunctions abnormally increases by reason of the enhancement interfacial coupling, while that of zigzag heterojunctions simply follows the normal decreasing trend. Furthermore, Liu *et al* [251] found that the interfacial thermal conductance of graphene/silicene decreases with increasing sample length, temperature and tensile strain, but is almost independent of the imposed heat flux, which could be understood based on the analysis of phonon spectra. It is worth noting that the imposed heat flux exceeds 42 GW m^{-2}, a low-frequency kinetic wave has been excited, providing an additional channel for the non-Fourier heat conduction at the interface.

As a kind of special graphene/h-BN hybrid structures, graphene/h-BN superlattices, have been predicted to possess many unusual physical properties such as high Seebeck coefficient and tunable bandgap [252, 253]. Meanwhile, the thermal conductivity in graphene/h-BN superlattices first decreases until it reaches a minimum value, and later it increases with the continuous increase of the period length. Here the minimum thermal conductivity corresponds to the crossover between coherent and incoherent phonon transport, as described in the previous chapters. For the typical 'superlattice characteristic', Zhu *et al* [254] explained that the initial reduction of thermal conductivity partially arises from the change of the phononic band structure induced by interfacial modulation, and the subsequent increase of thermal conductivity is ascribed to reduced inelastic interface scattering. Furthermore, they found that the coherent phonon transport in such superlattice is very sensitive to interfacial defects and superlattice periodicity disorder. Using SED approach, Silva *et al* [255] revealed that the phonons with frequencies up to 23 THz contributes 90% of the thermal conductivity in the graphene/h-BN superlattices, and the reduction of group velocities is the main reason of the monotonic decrease in the thermal conductivity as the period length increases. Additionally, Chen *et al* [256] showed that the period length corresponding to the minimum thermal conductivity will shift to lower values at higher temperatures and the coherent phonon transport is strengthened with decreasing temperature. As shown in figures 7(a)–(c), it can be seen that at 200 K, the thermal conductivities of graphene/h-BN superlattices with certain specific period lengths are very close to that at 300 K, against our common sense that the thermal conductivity of a superlattice generally decreases with increasing temperature. This anomalous thermal transport behavior was believed to be the result of strong phonon wave interference based on the analysis of phonon spectra. Analogously, Wang *et al* [257] calculated the thermal conductivity of graphene/nitrogenated holey graphene superlattice as a function of period length under different external conditions. The calculated results showed that the coherence length of such super lattice is 4.43 nm at room temperature and is independent of the sample length. Especially, at 100 K, the phonon wave interference becomes more remarkable, which enhances the coherence length and results in the occurrence of wave-like temperature profile.

4.2.2. van der Waals (Vdw) heterostructures. Vdw heterostructures have become a new research field because the vertically stacked structures possess a relatively cleaner interface for fundamental research and better device performance [258]. Besides, the presence of weak Vdw force may construct an isolated environment for parent 2D materials, regardless of the atomic commensurability. For graphene/h-BN Vdw heterostructures, experimental observations demonstrated that there are three different ways of stacking the unit cell of the two 2D materials, namely AA, AB and AB^+ configurations [259]. Since the lattice mismatch between graphene and h-BN is only 1.7%, the two pile together, forming a periodic moire pattern. Different moire pattern, depending on lattice mismatch and stacking misorientation, can affect the thermal transport properties of Vdw heterostructures. Jung *et al* [260] observed that the phonon dispersion relation of graphene/h-BN Vdw heterostructures for the AB stacking configuration is closer to that of gaphene, suggesting that the AB stacking configuration is more stable than the AA stacking configuration. Zhang *et al* [261] found that supported gaphene on a multilayer h-BN substrate exhibits high-performance heat dissipation. In detail, the thermal conductivity of h-BN-supported graphene was only decreased by 23% compared to that of the suspended case, much higher than the calculated value of the SiO_2 substrate. The underlying mechanisms were revealed that the smooth and atomically flat surface of h-BN substrate leads to weak stress distribution in gaphene, and has little influence on phonon relaxation time and mean free path in supported graphene. Moreover, it was found that the stacking faults or structure rotation could dramatically change the thermal conductivity of h-BN-supported graphene. Similarly, Pak *et al* [262] showed that the interfacial thermal conductance of graphene supported on h-BN is obviously superior to that of graphene on amorphous silica. This was possibly because the charge polarization throughout graphene that induces strong interlayer adhesion between graphene and h-BN. Zhou *et al* [263] noted that the h-BN substrate has little effect on the phonon group velocities of supported graphene by reason of weak interlayer interactions, but causes a considerable reduction of the lifetimes of ZA phonons owing to the invalidity of the selection rule. Based on NEGF method, Kumar *et al* [264] demonstrated in-plane acoustic modes have

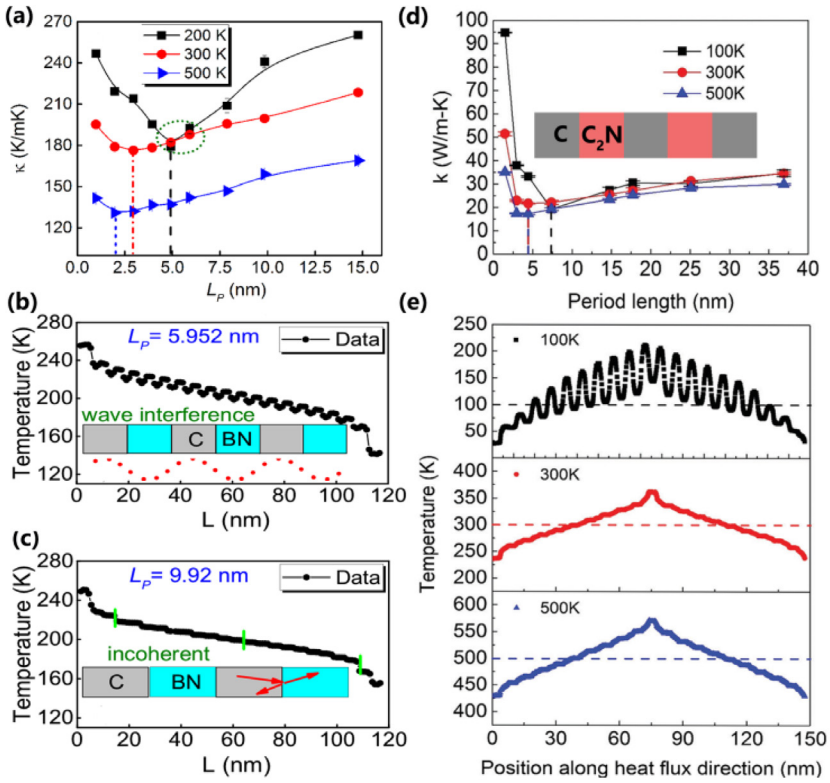

Figure 7. (a) The thermal conductivity of graphene/h-BN superlattice as a function of period length (L_p) at different temperatures. Temperature distribution of graphene/h-BN superlattice with (b) $L_p = 5.9252$ nm and (c) $L_p = 9.92$ nm at 200 K. (d) The thermal conductivity of pristine/nitrogenated holey graphene superlattice (C_2N) at different temperatures. (e) Temperature distributions along the heat flux direction of this superlattice with $L_p = 7.38$ nm at different temperatures of 100, 300 and 500 K. Note that when the temperature profile shows a wave-like behavior, it means that phonon wave interference plays an important role in phonon transport. Reprinted figures (a)–(e) with permissions from [256, 257], respectively. Copyright (2016) by AIP Publishing LLC and copyright (2017) by the PCCP Owner Societies.

the dominant contributions to thermal boundary conductance for Vdw graphene/h-BN heterojunctions with lower interfacial spacing. That is, as interfacial spacing increases, the relative contribution of the in-plane modes to the thermal conductance declines and the contribution of out-of-plane acoustic modes improve. Another important result in this paper is that the thermal conductance can be enhanced by more than 50% via regulating the lattice stacking arrangements. As shown in figure 8, Chen *et al* [265] designed a feasible experiment in which the thermal conductance at graphene/h-BN interfaces is measured using electrically heating means in combination with Raman spectroscopy technique. The measured results indicated that the thermal interface conductance of this junction is 7.4 MW K^{-1} m^{-2}, which is lower than those reported for graphene/SiO_2 and graphene/Au interfaces, but is higher than that reported for graphene/SiC interface. Besides graphene/h-BN Vdw heterostructures, Hong *et al* [266–268] successively studied the interfacial thermal transport across graphene/phosphorene, graphene/$MoSe_2$ and graphene/stanene Vdw heterostructures, and found their interfacial thermal conductance is ranging from 4 to 50 GW K^{-1} m^{-2}. Furthermore, Liu *et al* [269, 270] predicted that the interfacial thermal conductance of graphene/MoS_2 and graphene/silicene are about 5 GW K^{-1} m^{-2} and 10 GW K^{-1} m^{-2} at 300 K, respectively, which can be further modulated by the ambient temperature and interface coupling strength.

4.3. Carbon-based nanofillers

In electronic packaging, the introduction of TIM between the integrated circuits and the heat sink could eliminate the air gaps separating them, and enhanced the heat dissipation. For now, polymers as an important raw material have been widely used for TIM in modern electronic packages. In general, the thermal conductivity of bulk polymers is low, ranging from 0.1 to 0.5 W m^{-1} K^{-1} [271], because the morphology of the polymer chains has only the degree of short range order but no long-range order. Hence, it is natural to expect that the thermal conductivity of polymers can be enhanced by some controlling methods. Based on a two-stage heating method, Shen *et al* [272] observed that when the drawing ratio reaches 400, the thermal conductivity of polyethylene nanofiber is as high as 104 W · m^{-1} K^{-1} due to improved chain orientation under mechanical stretching. Using MD simulations, Yang *et al* [273] found that the thermal conductivity of polyethylene increases with the increasing strain, and the trend of thermal conductivity could be exponentially fitted with the orientation order parameter.

In addition to mechanical stretching, another common method to enhance the thermal conductivity of polymers is to incorporate highly thermal conductive fillers such as graphene and CNTs to create additional heat pathways, which has been demonstrated by numerous experimental studies [274–284]. In theory, Li *et al* [285] studied the effects of interfacial

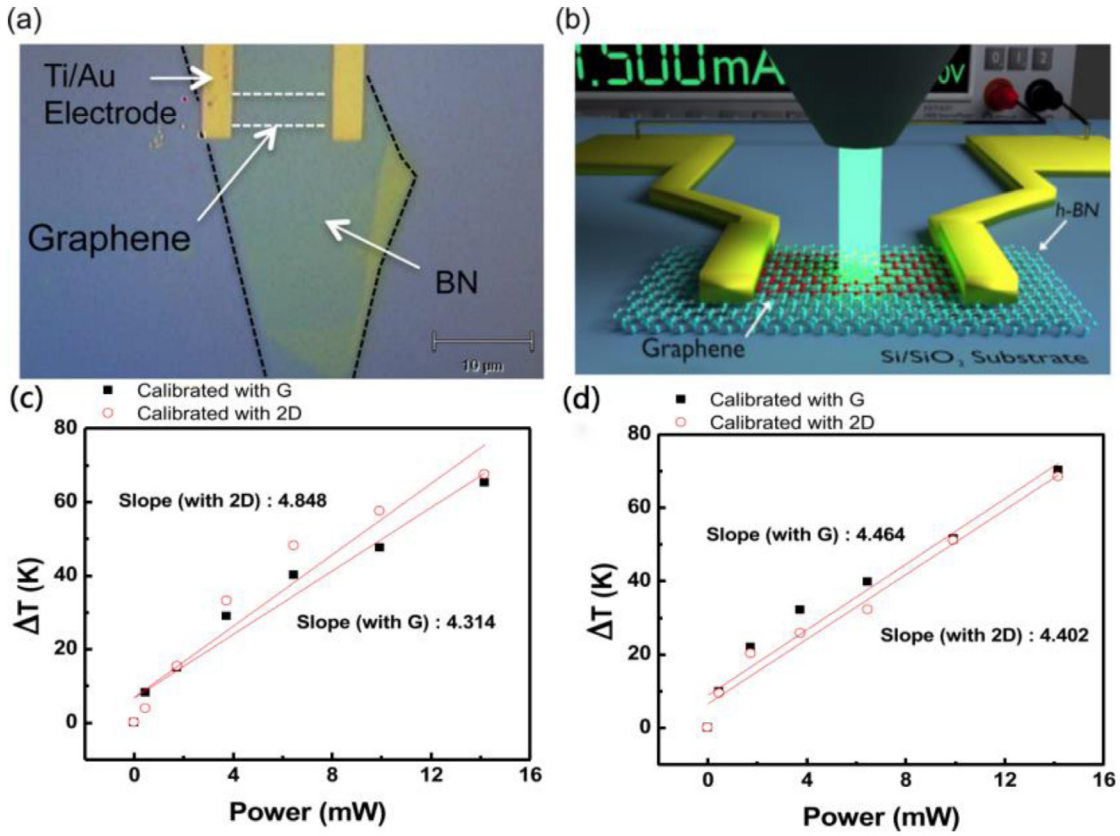

Figure 8. (a) Optical image and (b) schematic diagram of the graphene/h-BN Vdw heterojuction and experiment setup. Temperature difference across the interface of graphene/h-BN calibrated with 2D, G bands and BN optical phonon Raman frequencies of the (c) first and (d) second electrical heating. The slope of the curve normalized by the interface area ($A = 30\ \mu m^2$) is the interface thermal conductance ($G = Q/A\Delta T$). Reprinted with permissions from [265]. Copyright (2014) by AIP Publishing LLC.

SWCNT-matrix thermal resistance and volume fraction of SWCNT on the thermal conductivity of SWCNT-based polymer nanocomposites. The calculated results demonstrated that when the thermal resistance is smaller than the critical value of 2×10^{-7} Km^2 W^{-1}, the effective thermal conductivity of such nanocomposite increases with the volume fraction, while the thermal resistance exceeds the value, the thermal conductivity of system is lower than that of the pure polymer matrix. However, the existing acoustic or diffuse mismatch model, and MD simulations could not predicted accurately the interfacial thermal resistance between the filler and the polymer matrix under the actual circumstance, which are closely related with voids and molecule arrangement at the interfaces. As showed in figure 9, Haddon *et al* [282] experimentally found that the adoption of graphene-CNTs hybrid as nanofillers can achieve a synergistic effect in the thermal conductivity improvement of epoxy composites, which is ascribed to the formation of a more efficient percolating nanoparticle network. Meanwhile, it is reported that the additional CNTs play the role of nucleation agents, which improves the crystallization rate of polymer matrix, and increases the thermal conductivity of nanocomposites [286]. Moreover, the choice of larger fillers benefits the heat conduction in nanocomposites, but probably weakens other physical properties of system. In short, the thermal conductivity of carbon-based nanocomposites mainly depends on the following factors: the filler volume fraction, size-dependent thermal conductivity of the fillers, and interface coupling between fillers and polymer.

To further increase the thermal conductivity of carbon-based nanocomposites, surface functionalization as an effective way has been adopted to strength the coupling between the fillers and the polymers matrix, reducing the interfacial thermal resistance. Huang *et al* [287] found that the functionalization increases the thermal conductance at CNT-polymer interface by an order of magnitude compared to the non-functionalized case, because of the enhanced coupling between CNT and the matrix. It is worth noting that functionalization also decreases the intrinsic conductivity of CNTs due to increasing phonon scattering. More importantly, they noted that the introduction of graphene nanosheets without functionalization could remarkably increase the interfacial contact area with matrix polymers, and lowers the interfacial thermal resistance, which is very promising for taking the place of CNTs. Using MD simulations, Ni *et al* [288] found that although grafting of aromatic polymer onto the CNTs lowers the interfacial thermal resistance between the CNT and the surrounding polymer matrix, gives rise to a smaller effective thermal conductivity in the polymer composite. Wang *et al* [289] investigated systematically the influences of different non-covalent functional molecules including 1-pyrenebutyl, 1-pyrenebutyric acid and 1-pyrenebutylamine on the interfacial thermal resistance between graphene and polymer. It is

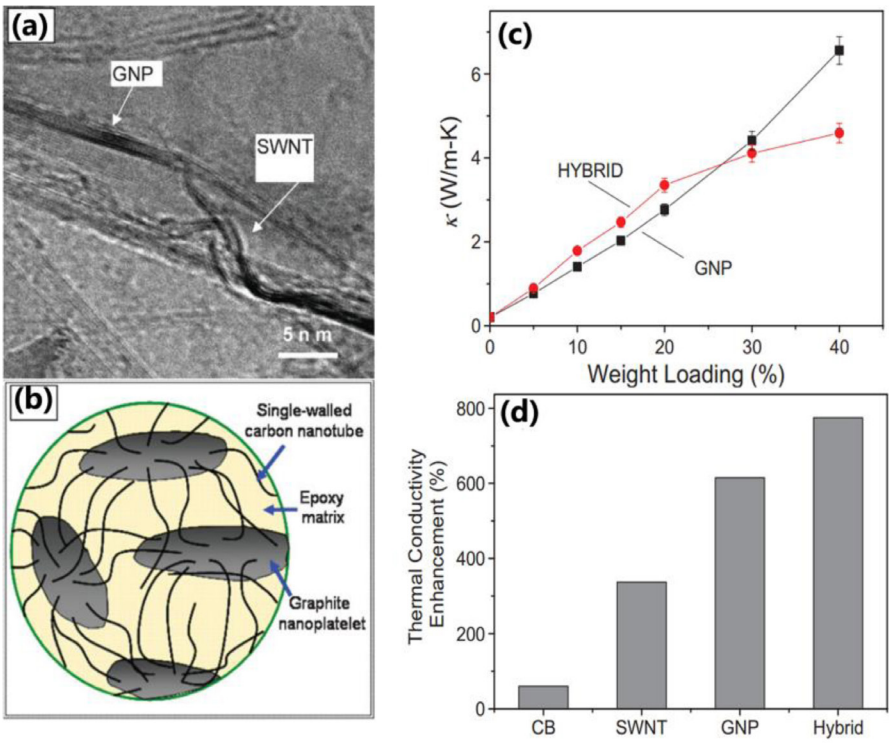

Figure 9. (a) Transmission electron microscope images of the cross-section of graphene-CNTs hybrid filler/epoxy composite. (b) Schematic representation of graphene-CNTs network in polymer matrix. (c) Thermal conductivity of epoxy composites with graphene-CNTs hybrid filler and graphene filler versus the filler loading. (d) Thermal conductivity improvement of epoxy composites for CNTs, graphene and graphene-CNTs hybrid filler at 10 wt% loading compared to carbon black. Reprinted with permissions from [282]. Copyright (2008) by WILEY-VCH Verlag GmbH & Co. KGaA, Weinheim.

found that the three functional molecules all produce similar reductions in the thermal resistance and the reduction magnitude depends on the volume fraction functional molecules. This is because the absorption of noncovalent functional molecules increases the overlap of the vibrational density of states between graphene and polymer. At the same time, the mechanical properties of such nanocomposites were not supposed to degenerate after adding these functional molecules. Similarly, by non-covalently functionalizing graphene surfaces, Lin *et al* [290] designed phonon-spectra linkers to bridge the vibrational mismatch at the graphene/organic interfaces, and showed the interfacial thermal conductance to be increased up to 120% using the C_8-pyrene linkers. Kim *et al* [291] found that the functionalization of graphene enhances the thermal conductivities of graphene/polymer composites for fillers with smaller size, while the graphene size exceeds a critical value, the situation reversed. The reason for this phenomenon was that functionalization promotes the thermal transport at graphene-polymer interface, but reduces the intrinsic thermal conductivity of grapheme similar to that in graphene-based nanofluids [292]. Gao *et al* [293] showed that there is maximum thermal conductivity of graphene/polymer composites at an intermediate grafting density because as the grafting density increases, the thermal conductivity perpendicular to the graphene plane rises linearly, but the in-plane thermal conductivity of graphene drops sharply. Besides the optimal grafting density, there also existed an optimal balance between grafting density and grafting length to obtain the maximum enhancement for the parallel thermal conductivity. In particular, Li *et al* [294] systematically investigated the effect of different types of defects on the interfacial thermal transport between the gaphene and polymer using NEMD simulations and the effective medium theory. It is found that the presence of Stone-Wales and Multi-vacancy defects can increase the interfacial thermal conductance. For instance, as the fraction of SW defect ranged from 0% to 13%, the interfacial thermal conductance increased from about 135.5 to about 162.6 MW K^{-1} m^{-2}. It was explained that the phonon spectra of defective graphene sheet has better matching degree with that of the epoxy matrix especially at the low-frequency modes, facilitating the interfacial thermal transport.

5. Applications range

5.1. Thermal management

From the prospective of informatics, phonons might be used similarly to electrons in electronics and photons in photonics as carriers of information for data processing in the emerging field of phononics. As stated in the introduction section, a series of thermal devices [33–36] analogous to the electronic counterparts have already been conceptualized. Then, these concepts have been gradually implemented in realistic nanomaterials by adopting various design configurations. Up to now, some models of thermal devices have been prepared in experiment. For example, the successful preparation of thermal memory device would promote the development of smart thermal management [295]. Note that TR and NDTR are the fundamental

components for realizing functional thermal devices. Here, TR is an asymmetric heat transfer phenomenon in which heat can be conducted easily in one direction but much harder in the opposite direction, and NDTR is that the heat flux decreases as the applied temperature difference increases.

The controllable thermal conductivity of carbon-based low-dimensional nanostructures provides outstanding testing platform not only for heat dissipation application but also for manipulating heat signals. Up to now, numerous theoretical and experimental works have studied current rectification and NDR in carbon nanomaterials and have obtained lots of meaningful results [63–65]. However, phonons as a quasi-particle distinguishing from electrons are hard to manipulate directly by the electromagnetic field. To obtain the optimal TR ratio, several structural models have been proposed to construct nanoscale thermal rectifiers, including asymmetric nanoribbons, nanojunctions, graded nanowires, and phase change materials. Among them, graphene/CNTs-based thermal diodes are expected to possess high TR ratio and fast response speed because of the large phonon group velocity, and might be applied in logic calculations performed with phonons. Wu *et al* [45] found that the thermal transport in carbon nanohorn exhibits obvious asymmetry (namely TR effect) before and after reversing the temperature bias, and the value of TR ratio strongly depends on the system size, temperature bias and tensile loading. Ni *et al* [296] designed the thermal rectifiers based on partially unzipped CNTs, and showed that the TR ratio in such junctions could reach 140% under a large temperature bias of 300 K, which may be well-suited for phononics application. Under the same conditions, Yang *et al* [297] reported a large TR ratio of 350% in trapezia-shaped GNRs with 4.2 nm length, outperforming that of graded InAs nanowires [298]. Moreover, using NEGF method, Xie *et al* [299] investigated the nonlinear phonon transport properties in asymmetric graphene-based three terminal junctions. The simulated results showed that the TR effect is apparent in the junctions and is able to be further enhanced by increasing the asymmetric degree or the width of central terminal. Ruan *et al* [300] pointed out that TR effect is often notable in nanosized asymmetric GNRs, but diminishes at larger width. The origin of TR was considered to be that induced the edge effects of phonons (also known as phonon lateral confinement) causes several possible mechanisms for TR, which includes the mismatch of phonon spectra, inseparable dependence of κ on temperature and space, and phonon edge localization. Furthermore, constructing asymmetric structural defects in GNRs also obtain remarkable TR effect. For example, Wang *et al* [301] studied the TR effect in asymmetrically defected GNR and showed that SV and Si defects are more favorable to enhance the TR efficiency than that DV and SW defects. Also, they concluded that the optimum conditions for TR include low temperature, high temperature bias, moderate concentration of defects, and short system length. Recently, a similar conclusion has been obtained by experimental studies in asymmetrically defected GNR [302], as shown in figure 10.

Besides, asymmetrically functionalized molecular is another effective method to enhance the TR ratio in carbon-based nanomaterials. Allaei *et al* [303] found that the thermal resistance at pristine/hydrogenated CNT interfaces strongly depends on the direction of heat flux, namely, existing TR effect. Under a tiny temperature bias of 20 K, the TR ratio could achieve 35%, and further regulation for TR effect could be made by altering tube diameter and hydrogen coverage. Tang *et al* [304] investigated the TR effect in pristine/silicon-functionalized GNRs and observed that a moderate Si/C ratio and patterned arrangement are helpful to obtain a higher TR ratio. In addition, they also observed that the TR ratio is positive correlation to temperature bias, but negative correlation to the environmental temperature and sample length. Pal *et al* [305] presented a scheme to enable higher TR ratio using polymer-functionalized CNTs and showed that the TR ratio of such composite structure is up to 204% under a temperature bias of 40 K. This work also determined two necessary conductions for realizing TR in nanostructures: one is structural asymmetry and the other is changing the temperature-dependent feature of phonon spectra. Melis *et al* [306] designed three types of thermal rectifiers based on graphene/graphene interfaces with vertical, triangular, and T-shaped morphologies, and identified the best TR performance (about 54%) in the triangular one. Also, they explored the dependence of the TR ratio on the system size, vertex angle, and temperature gradient. On the other hand, constructing carbon-based nanojunctions is another popular approach to realize high-effectively TR. The difference of material at the two sides of heterojunctions normally leads to the asymmetry of phonon scattering, which is also the principle of TR. Chen *et al* [307] designed a thermal rectifiers based on carbon/boron nitride heteronanotubes (ACBNNTs) and obtain as high as 334% TR ratio in such heterojunctions under a temperature bias of 300 K, indicating promising application in high-efficiency thermal rectifier. Furthermore, they found the optimum conductions for high TR efficiency, including large temperature bias, low temperature, small system size, low defect density, weak substrate interaction and small strain tensile. With the help of wave packet dynamics simulation and power spectrum calculation, the underlying mechanism of TR was considered that the strong coupling between low-frequency transverse phonons across the interface in the direction of reverse large bias. Similar phenomena have been observed in graphene/h-BN nanoribbons (CBNNRs) [308, 309]. Sandonas *et al* [310] studied the influence of substrate deposition on the thermal transport properties of CBNNRs and found a reduction of the interface thermal resistance in the heterojunctions upon substrate deposition because of an increment of the overlap between the phonon spectra of graphene and h-BN domains. More importantly, it was demonstrated that the TR ratio increases with the level of structural asymmetry for BNCNRs, being up to ~24%, and can be further improved by varying the substrate temperature. Recently, Cao *et al* [311, 312] designed the thermal rectifiers based on graphene-CNTs junction, and showed the maximum TR ratio could be up to 1200%, which is closer to the practical application requests. By the analyses of power spectrum, the mechanism for the ultrahigh TR ratio was that the formation of the standing wave (a kinetic wave) only appears in the heat flux direction from the tube to the GNR end. Commonly, once a kinetic wave is excited,

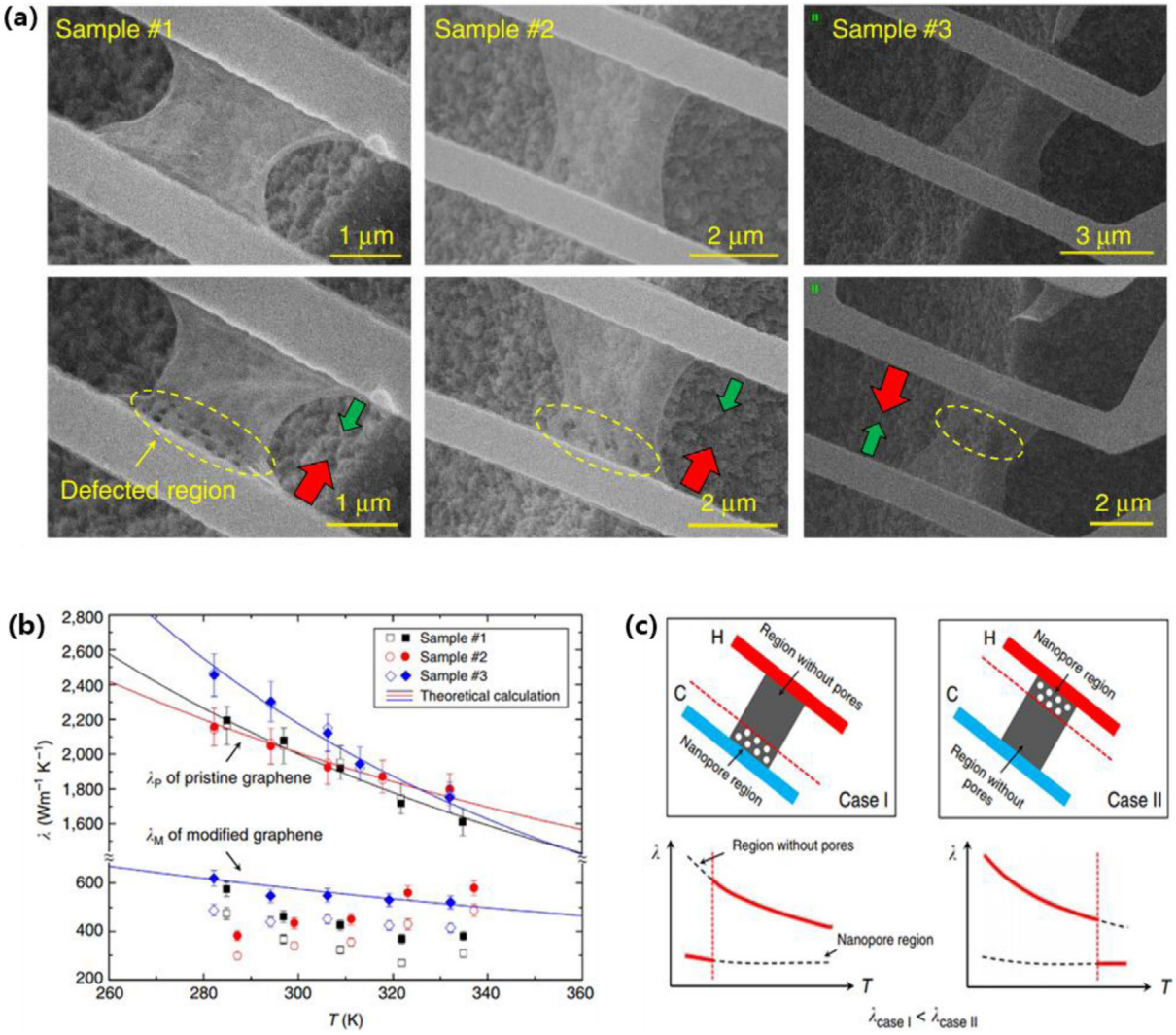

Figure 10. (a) Scanning electron microscopy images of graphene before and after defect engineering. (b) Thermal conductivities of graphene samples (#1–#3). Obviously, the measured thermal conductivity of pristine graphene is almost independent of the direction of heat flux (solid and open symbols). However, for the graphene after defect engineering, the measured thermal conductivity λ was larger in the direction of heat flux from the defective region to the pristine region (solid symbols) than that in the opposite direction (open symbols). (c) Explanation of the physical mechanism for the TR. Reprinted with permissions from [302]. Copyright (2017) by Nature Publishing Group.

there accordingly exists a sharp peak in the power spectra and the wave-dominated energy mechanism (namely non-Fourier heat conduction) rather than the traditional Fourier conduction will play a significant role in thermal transport process. Similar conclusions have been achieved in previous studies [251, 298, 307, 308]. Sometimes, the wave-dominated energy mechanism could provide an additional channel for interfacial thermal transport in certain nanostructures. It is worth noting that the excitation of kinetic wave often needs large temperature or high heat flux, and is closely related with the length of sample. Tuo *et al* [313] designed a bimaterial fiber thermal rectifier by connecting a crystalline polymer nanofiber (PE) to a cross-linked polymer nanofiber (PEX) and the working principle is as follows: when the temperature gradient is established, the linear PE portion undergoes phase transition while the PEX portion does not, thus resulting in a remarkable variation of thermal conductivity and a TR ratio of about 100% under smaller temperature. Cottrill *et al* [314] presented the concept of dual phase change thermal diode (DPCTD) based on a junction between two phase change materials with opposing thermal conductivity trends as a function of temperature, and predicted that the TR ratio of this thermal diode has obviously positive correlation with the square root of the ratio between the thermal conductivity of two constituent materials. Guided by the theoretical result, a DPCTD based on octadecane-impregnated polystyrene foam was fabricated, and the measured TR ratio was up to 160%, in line with the proposed theoretical equation.

Apart from TR effect, NDTR as another vital physical phenomenon plays an important role in the operation of thermal devices such as thermal transistor, thermal switch and thermal amplifier. As shown in figure 11, Chen *et al* [315] observed that in graphene/h-BN heterojunctions, when the applied temperature bias surpasses a threshold, the system

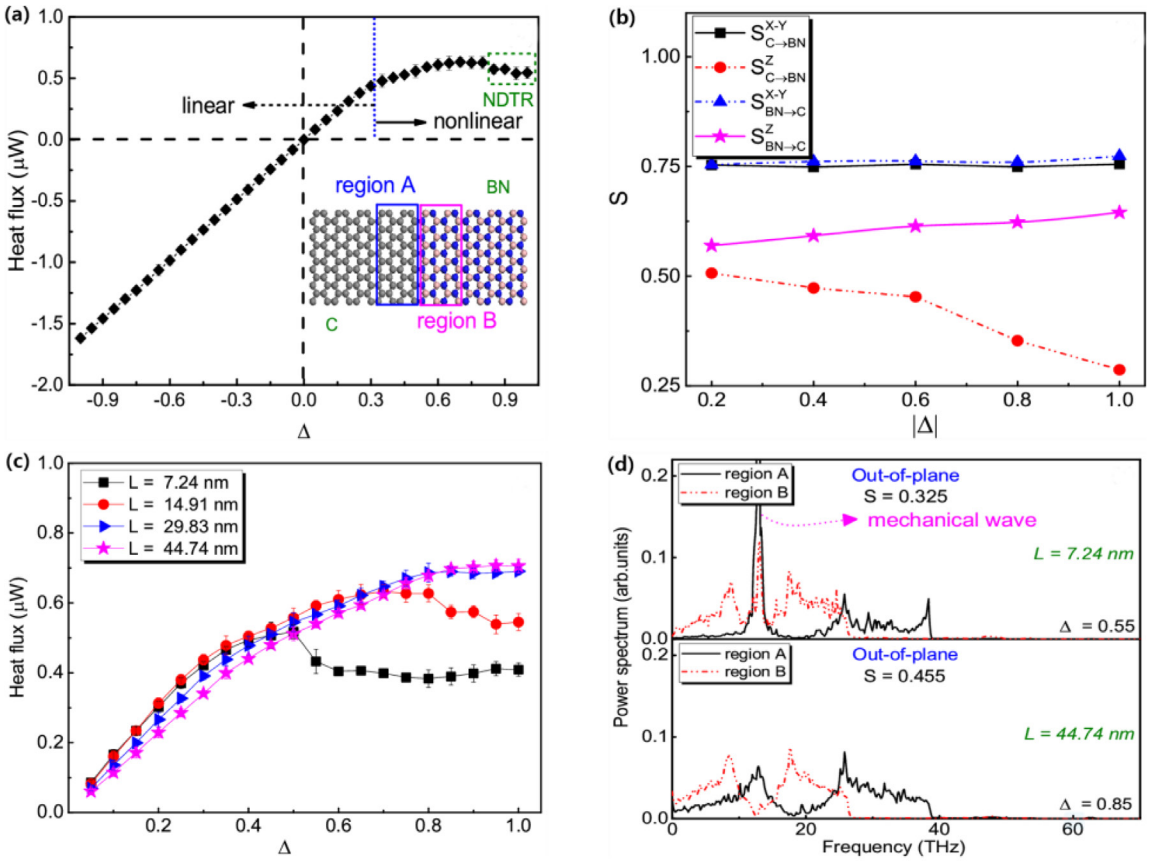

Figure 11. (a) Heat flux J as a function of normalized temperature difference Δ for the graphene/h-BN heterojunctions. Here, $T_L = 500$ K and T_R is varied from 480 K to 100 K. (b) The matching coefficients S between the in-plane/out-of-plane power spectra of graphene and h-BN regions as a function of Δ. The dependence of (c) NDTR and (d) out-of-plane spectra on the system width. Reprinted with permissions from [315]. Copyright (2017) by AIP Publishing LLC.

enters nonlinear response regime, where NDTR may appear. This is because under large temperature bias, the excitation of out-of-plane acoustic wave only appears in graphene domain, and it leads to an obvious mismatch between the lattice vibrations of graphene and h-BN domains, impeding thermal transfer across interface. Ai *et al* [316] found that there exists remarkable NDTR behavior in pure CNTs, and the regime of NDTR becomes smaller and eventually vanishes with increasing the tube length. Additionally, double NDTRs even appear for some diameters of CNTs. Puri *et al* [317] designed a thermal AND composed of using two identical thermal rectifiers based on asymmetric GNRs. By performing logic calculations with phonons, the performance of this AND gate has been tested. That is, when either input was at a logic 0 state, the device output parameter ε ranged from 0 to 0.275, approaching that for a typical silicon based electrical diode ($0 \leqslant \varepsilon \leqslant 0.12$). In addition, the switching speed of the AND gate was 100 ps as well as that in fast electrical diodes, which stems from the fast phonon propagation speed in graphene. Zhong *et al* [318] reported that the three-terminal GNRs can realize some functions of thermal devices such as thermal valve, thermal switch and thermal amplifier, indicating GNRs have great potential in controlling the flow of heat at nanoscale.

5.2. Thermoelectric conversion

Thermoelectric materials can generate electricity directly from waste heat, which are crucial in renewable energy conversion to solve the global energy crisis. The energy conversion efficiency of thermoelectric materials is determined by the dimensionless figure of merit ZT, which is defined as

$$\mathrm{ZT} = \frac{\sigma S^2 T}{\kappa_e + \kappa_p} \tag{22}$$

where σ is the electrical conductivity, S is the Seebeck coefficient, T is temperature, κ_e and κ_p is respectively the electronic and phonon thermal conductivity. In general, when the value of ZT is greater than 3, thermoelectric power generator would become competitive with traditional power generators. So far, commercial thermoelectric materials ranging from low temperature to high temperature mainly include Bi_2Te_3, $CoSb_3$, PbTe, and SiGe and the maximum ZT value of these commercially available thermoelectric materials is around 1.0 [148]. Hence, for the practical viability of thermoelectric applications, it is necessary to enhance the converting efficiency of thermoelectric materials. However, in bulk materials, increasing the ZT value is not a simple

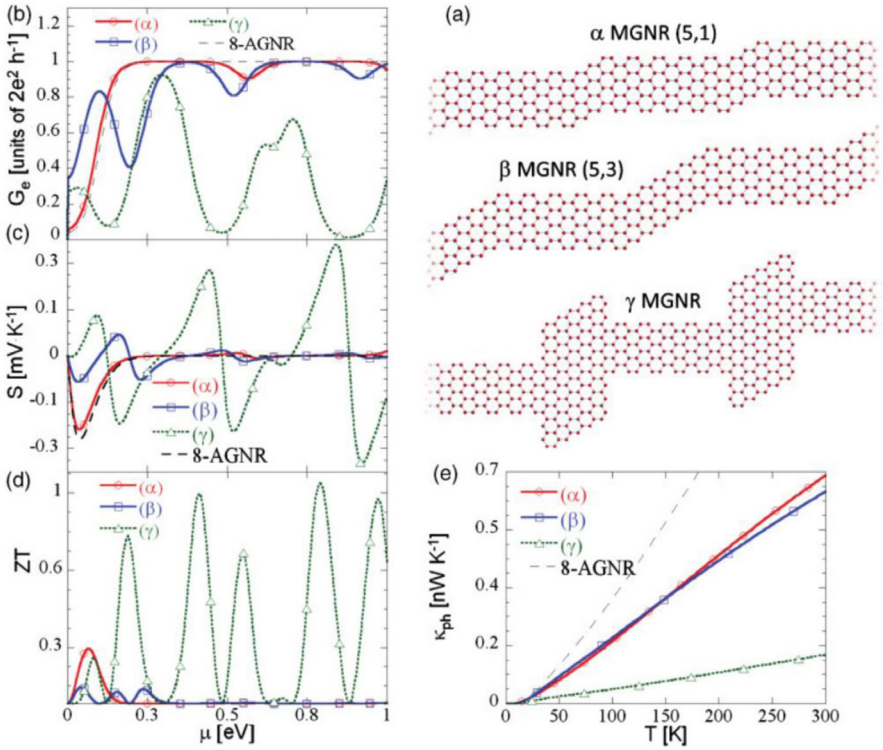

Figure 12. (a) Schematic view of MGNR with different configurations (α, β and γ). (b) Electronic conductance, (c) Seebeck coefficient, and (d) ZT value as a function of chemical potential μ. (e) phonon thermal conductance versus the temperature for different GNR structures. Reprinted with permissions from [321]. Copyright (2011) by American Physical Society.

process, because the factors affecting thermoelectric performance are intrinsically coupled so that it is hard to control them independently.

In 1993, Hicks *et al* [319] firstly proposed that nanostructuring materials might provide much better thermoelectric efficiencies than that in bulk materials. There are two reasons for the enhancement of ZT value in low-dimensional nanomaterials: (1) the increase of Seebeck coefficient owing to size-quantization; (2) the reduction of lattice thermal conductivity caused by phonon boundary scatterings. It is well known that carbon nanomaterials possess many fascinating properties such as unique electrical structure and thermal performance because of the diversity of their structures, demonstrating promising potential for thermoelectric applications. Using the NEGF method combing with the tight-binding model, Xie *et al* [320] found that the ZT value of ZGNRs with stub structures could achieve 0.26 at room temperature and can be improved via tuning the geometric parameters of the stub. The large ZT value was partly ascribed to the lower phonon thermal conductance in GNRs junctions. The more important was that the fluctuation of electronic transmissions within the first conductance band substantially improves the Seebeck coefficient. As shown in figure 12, Mazzamuto *et al* [321] prospered a mixed GNR (MGNR) model constructed by alternating armchair and zigzag sections of different width and studied the thermoelectric performance of this mixed GNR. The obtained results demonstrated that the ZT value of some optimized GNR structures is as high as 1 at small chemical potential. One of important reasons for the large ZT value was that the strong resonant tunneling effect of electrons between armchair and zigzag sections retains high electron conductance, and enhances Seebeck coefficient.

Moreover, Liang *et al* [322] investigated the thermoelectric properties of several kink GNRs that have been successfully synthesized using a surface-assisted bottom-up chemical approach, and revealed that the significant improvement ZT value in these GNRs is due to that the phonon thermal conductance is dramatically degraded while the electronic conduction is preserved due to the resonant tunneling effect. Yokomizo *et al* [252] found that the Seebeck coefficients of the graphene/h-BN superlattices are 20 times larger than that of graphene and are very sensitive to the proportion of h-BN. Similarly, Tran *et al* [323] studied the thermoelectric properties of GNRs with branched BNNRs on the side surfaces. The advantage of such branched GNRs is that phonon conductance could be greatly reduced because of the vibrational mismatch between GNRs and BNNRs sections, while the electron transmission is weakly affected. The calculated results showed that the ZT value in pure branched GNRs reach 0.8 and could be further raised to 1.48 by introducing appropriately vacancies in the channel.

Another efficient way to enhance the thermoelectric performance of carbon nanomateirals is to sharply reduce their thermal conductivities. In particular, Zhou *et al* [206] observed that the ZT value of defective β-graphyne nanoribbons is as high as 1.64, far more than that of pure ones, which can be ascribed to the strong phonon-defect scattering and the intensive localization of phonons. In addition, introducing anti-dots

in the interior in the interior of ZGNRs has little influence on the currents distributed nanoribbon edges, but drastically reduces the system's phonon thermal conduction [324]. As a result, the ZT value of 1 μm-length GNRs still achieved 5 at room temperature by controlling the arrangement and the diameter of nanopores. Tan *et al* [325] constructed a ZGNRs/gold chains/ZGNRs model (called An), and found the phonon conductance of An is only 5% of that pure ZGNRs at room temperature, and the electronic transmission near the Fermi level retains owing to the fact that there are edges for the electrons transport. Consequently, the room-temperature ZT value of An could be over 1. Nguyen *et al* [326] investigated the thermoelectric properties of Vdw graphene junction, and showed that the phonon conductance of this junction is reduced by 92% compared to that of single graphene layer because of the presence of weak Vdw interactions. Meanwhile, the electronic performance was less affected. Based on this strategy, the obtained ZT value could easily exceed 1, and be further promoted to 3.4 at 600 K by inserting adding periodic nanoholes in the bottom graphene sheet. Ouyang *et al* [327] investigated the influence of edge disorder on the thermoelectric performance of γ-graphyne nanoribbons. The calculated results showed that the thermal conductance is strongly suppressed by the dissociation of edge acetylenic linkages, but the Seebeck coefficient is almost unaffected by this factor. Hence, the ZT value of this γ-graphyne nanoribbon with 55.68 nm length and 1.41 nm width was able to approach 2.5 at room temperature. With the progressing of molecular synthetic technique, various organic single-molecules and some novel nanostructures have been designed and showed excellent electronic [328–332] and thermal properties [333–336]. Meanwhile, molecular junctions were expected to serve as the powerful thermoelectric materials. Bürkle *et al* [337] systematically studied the thermoelectric properties of paracyclophane-based single-molecule junctions with gold electrodes and observed that the thermopower of such single-molecule junctions can be flexibly tuned by adsorbing different functional groups. Cao *et al* [338, 339] confirmed that the phonon thermal conductance of molecular devices is largely reduced compared with that of zigzag GNRs. The calculated ZT value was optimized to be 1.4 at 300 K by adjusting the coupling between molecule and electrodes. Some recent studies on the thermal and thermoelectric transport in molecular junctions have also been reported [340–342]. It should be pointing out that, the effect of electron–phonon interaction is normally neglected in most previous theoretical studies on thermoelectric materials though it may has significant effect on the electron transport of nanostructures. Recently, it was found that the performances of spin filter and magnetoresistances in GNRs obviously degrade when considering the electron–phonon coupling [343, 344]. Specially, Li *et al* [345] found that in GNRs, the inelastic currents primarily contributed by several low-energy in-plane phonons are about two times than the elastic ones under higher temperature, and could improve the spin-dependent Seebeck effect. Note that the present theory of electron–phonon interaction is not in exact consistency with experiment results, and needs to be further improved.

6. Conclusions and outlook

In this review, we first introduced several kinds of experimental techniques and theoretical approaches which investigates the thermal transport properties of different carbon nanostructures, and discussed possible physical mechanisms for the observed transport phenomenon related to the low-dimensional nature of phonons such as size dependence, quantum effect, and anisotropic feature. Moreover, some basic thoughts to manipulate the thermal transport in carbon nanostructures have clearly been presented here. For example, the introduction of structural defects, Vdw interacation, functionalization and stress field usually enhances diffuse (particle-like) phonon scattering for a limited range of high-frequency phonons; while phonon interference or phonon local resonance induced by constructing supperlattice or branched structures can effectively control the low-frequency phonons; the mechanism of phonon bridge is widely used to enhance thermal transport across the interface between fillers and polymers. Note that most of results and predictions discussed in this paper are not verified by experiments, but it does demonstrate clearly that carbon nanomaterials may be very promising for future development of thermal devices and thermoelectric energy conversion.

Although systematical investigations from both experimental and theoretical efforts have been made to understand the physical mechanisms governing heat conduction in carbon nanomaterials, several questions and challenges remain. It is well known that phonons in a wide range of frequencies contribute to heat conduction. The multi-scale character of phonon transport usually leads to the difficulty in precisely determining that which phonons are scattered in the manipulation of thermal conductivity. Many other important questions are still not clear.

(1) The accurate description of different scattering mechanisms such as phonon-interface scattering, phonon-impurity scattering, electron–phonon scattering is still lacking. In particular, our understanding of electron–phonon scattering is still in the primary stage of development, with most treatments being based on the assumption that low-energy phonons are scattered by electrons, also not being verified in experiment. In addition, it is not clear to the intrinsic relevance among different phonon scattering mechanisms, and between them and phonon wave effect. Consequently, when manipulating the thermal conductivity of carbon nanomaterials by external factors, it is difficult to quantitatively distinguish the contribution from various kinds of transport mechanisms to the variation of thermal conductivity.

(2) As mentioned above, when the anomalous thermal transport appears in low-dimension carbon nanostructures, it normally accompanies the excitation of the kinetic wave—a transport of heat in the form of a wave, which differs from conventional acoustic wave that is a periodic fluctuation of mass density and pressure. Moreover, the smaller the system we studied, the more pronounced the kinetic wave becomes. It would be interesting to determine the contribution ratio from the non-Fourier transport to thermal conductivity based on experimental measurement.

(3) The primary challenge from the perspective of experiment lies in the difficulty of measuring the thermal contact resistance and detecting the temperature distribution at the micro-/nanoscale with high sensitivity. Also, the fabrication of desired low-dimensional carbon nanostructures is quite challenging.

Acknowledgments

This work was supported by the National Key Research and Development Program of China (No. 2017YFB0701602), by the National Natural Science Foundation of China (Nos. 11674092 and 11904161), by Hunan Provincial Natural Science Foundation of China (2018JJ3421), by the Scientific Research Fund of Hunan Provincial Education Department (18C0454).

ORCID iDs

Xue-Kun Chen https://orcid.org/0000-0003-3546-2443
Ke-Qiu Chen https://orcid.org/0000-0001-8627-0498

References

[1] Kroto H W, Heath J R, O’Brien S C, Curl R F and Smalley R E 1985 *Nature* **318** 162
[2] Lijima S 1991 *Nature* **354** 56
[3] Novoselov K S, Geim A K, Morozov S V, Jiang D, Zhang Y, Dubonos S V, Grigorieva I V and Firsov A A 2004 *Science* **306** 666
[4] Jin C, Lan H, Peng L, Suenaga K and Iijima S 2009 *Phys. Rev. Lett.* **102** 205501
[5] Castro Neto A H, Guinea F, Peres N M R, Novoselov K S and Geim A K 2009 *Rev. Mod. Rhys.* **81** 109
[6] Avouris P 2010 *Nano Lett.* **10** 4285
[7] Ning F, Wang D, Feng Y X, Tang L M, Zhang Y and Chen K Q 2017 *J. Mater. Chem.* C **5** 9429
[8] Balandin A A, Ghosh S, Bao W, Calizo I, Teweldebrhan D, Miao F and Lau C N 2008 *Nano Lett.* **8** 902
[9] Seol J H *et al* 2010 *Science* **328** 213
[10] Faugeras C, Faugeras B, Orlita M, Potemski M, Nair R R and Geim A K 2010 *ACS Nano* **4** 1889
[11] Chen S *et al* 2011 *ACS Nano* **5** 321
[12] Yu Y J, Han M Y, Berciaud S, Georgescu A B, Heinz T F, Brus L E, Kim K S and Kim P 2011 *Appl. Phys. Lett.* **99** 183105
[13] Dresselhaus M S, Dresselhaus G and Saito R 1995 *Carbon* **33** 883
[14] Thostenson E T, Ren Z and Chou T W 2001 *Compos. Sci. Technol.* **61** 1899
[15] Berber S, Kwon Y K and Tománek D 2000 *Phys. Rev. Lett.* **84** 4613
[16] Khoshnevis H, Mint S M, Yedinak E, Tran T Q, Zadhoush A, Youssefi M, Pasquali M and Duong H M 2018 *Chem. Phys. Lett.* **693** 146
[17] Liu P *et al* 2018 *Nano Today* **21** 18
[18] Deng Y X, Chen S Z, Zeng Y, Zhou W X, Tang L M and Chen K Q 2018 *Org. Electron.* **63** 310
[19] Cao L, Li X, Jia C, Liu G, Liu Z and Zhou G 2018 *Carbon* **127** 519
[20] Chen T, Li Q, Xu L, Zhang Y, Xu Z, Zhang Y, Wang L and Long M 2019 *Org. Electron.* **65** 49
[21] Sevinçli H and Sevik C 2014 *Appl. Phys. Lett.* **105** 223108
[22] Jiang P H, Liu H J, Cheng L, Fan D D, Zhang J, Wei J, Liang J H and Shi J 2017 *Carbon* **113** 108
[23] Hwang H J, Koo J, Park M, Park N, Kwon N Y and Lee H 2013 *J. Phys. Chem.* C **117** 6919
[24] Kou J, Zhou X, Lu H, Wu F and Fan J 2014 *Nanoscale* **6** 1865
[25] Yu H, Du A, Song Y and Searles D J 2013 *J. Phys. Chem.* C **117** 21643
[26] Fitzgibbons T C, Guthrie M, Xu E S, Crespi V H, Davidowski S K, Cody G D, Alem N and Badding J V 2015 *Nat. Mater.* **14** 43
[27] Zhang S, Zhou J, Wang Q, Chen X, Kawazoe Y and Jena P 2015 *Proc. Natl Acad. Sci. USA* **112** 2372
[28] Wang Z, Zhou X F, Zhang X, Zhu Q, Dong H, Zhao M and Oganov A R 2015 *Nano Lett.* **15** 6182
[29] Krainyukova N V and Zubarev E N 2016 *Phys. Rev. Lett.* **116** 055501
[30] Boukai A I, Bunimovich Y, Tahir-Kheli J, Yu J K, Goddard Iii W A and Heath J R 2008 *Nature* **451** 168
[31] Markussen T, Jauho A P and Brandbyge M 2009 *Phys. Rev.* B **79** 035415
[32] Chen Y, Jayasekera T, Calzolari A, Kim K W and Buongiorno Nardelli M 2010 *J. Phys.: Condens. Matter* **22** 372202
[33] Terraneo M, Peyrard M and Casati G 2002 *Phys. Rev. Lett.* **88** 094302
[34] Li B, Wang L and Casati G 2006 *Appl. Phys. Lett.* **88** 14350
[35] Wang L and Li B 2007 *Phys. Rev. Lett.* **99** 177208
[36] Wang L and Li B 2008 *Phys. Rev. Lett.* **101** 267203
[37] Balandin A A 2011 *Nat. Mater.* **10** 569
[38] Maruyama S 2003 *Microscale Thermophys. Eng.* **7** 41
[39] Maruyama S 2002 *Physica* B **323** 193
[40] Shiomi J and Maruyama S 2008 *Japan. J. Appl. Phys.* **47** 2005
[41] Chang C W, Okawa D, Garcia H, Majumdar A and Zettl A 2008 *Phys. Rev. Lett.* **101** 075903
[42] Xu X *et al* 2014 *Nat. Commun.* **5** 3689
[43] Wu G and Li B 2007 *Phys. Rev.* B **76** 085424
[44] Yang N, Zhang G and Li B 2008 *Appl. Phys. Lett.* **93** 243111
[45] Wu G and Li B 2008 *J. Phys.: Condens. Matter* **20** 175211
[46] Shao Z G, Ai B Q and Zhong W R 2014 *Appl. Phys. Lett.* **104** 013106
[47] Hu J, Wang Y, Vallabhaneni A, Ruan X and Chen Y P 2011 *Appl. Phys. Lett.* **99** 113101
[48] Barreiro A, Rurali R, Hernández E R, Moser J, Pichler T, Forro L and Bachtold A 2008 *Science* **320** 775
[49] Chang T, Zhang H, Guo Z, Guo X and Gao H 2015 *Phys. Rev. Lett.* **114** 015504
[50] Fthenakis Z G and Tománek D 2012 *Phys. Rev.* B **86** 125418
[51] Marconnet A M, Panzer M A and Goodson K E 2013 *Rev. Mod. Phys.* **85** 1295
[52] Al Taleb A and Farías D 2016 *J. Phys.: Condens. Matter* **28** 103005
[53] Xu X, Chen J and Li B 2016 *J. Phys.: Condens. Matter* **28** 483001

[54] Nika D L and Balandin A A 2013 *J. Phys.: Condens. Matter* **24** 233203
[55] Nika D L and Balandin A A 2017 *Rep. Prog. Phys.* **80** 036502
[56] Gu X, Wei Y, Yin X, Li B and Yang R 2018 *Rev. Mod. Phys.* **90** 041002
[57] Zeng Y J, Liu Y Y, Zhou W X and Chen K Q 2018 *Chin. Phys.* B **27** 036304
[58] Lu Z and Ruan X 2019 *ES Energy Environ.* **4** 5
[59] Xie Z X, Zhang Y, Yu X, Li K M and Chen K Q 2014 *J. Appl. Phys.* **115** 104309
[60] Xie Z X, Liu J Z, Yu X, Wang H B, Deng Y X, Li K M and Zhang Y 2015 *J. Appl. Phys.* **117** 114308
[61] Xie Z X, Zhang Y, Yu X, Wang H B, Li K M, Pan C N and Chen Q 2015 *J. Phys.: Condens. Matter* **27** 095303
[62] Taylor J, Guo H and Wang J 2001 *Phys. Rev.* B **63** 245407
[63] Fan Z Q and Chen K Q 2010 *Appl. Phys. Lett.* **96** 053509
[64] Zeng J, Chen K Q, He J, Zhang X J and Sun C Q 2011 *J. Phys. Chem.* C **115** 25072
[65] Chen T, Guo C, Xu L, Li Q, Luo K, Liu D, Wang L and Long M 2018 *Phys. Chem. Chem. Phys.* **20** 5726
[66] Mingo N and Yang L 2003 *Phys. Rev.* B **68** 245406
[67] Wang J S, Zeng N, Wang J and Gan C K 2007 *Phys. Rev.* E **75** 061128
[68] Xu Y, Chen X, Gu B and Duan W 2009 *Appl. Phys. Lett.* **95** 233116
[69] Peng X F and Chen K Q 2014 *Carbon* **77** 360
[70] Xie Z X, Chen X K, Yu X, Zhang Y, Wang H B and Zhang L F 2017 *Sci. China* **60** 107821
[71] Yang Z, Ji Y L, Lan G, Xu L C, Wang H, Liu X and Xu B 2016 *J. Phys. D: Appl. Phys.* **49** 145102
[72] Huang H 2015 *J. Phys.: Condens. Matter* **27** 305402
[73] Gorjizadeh N, Farajian A A and Kawazoe Y 2011 *J. Phys.: Condens. Matter* **23** 075301
[74] Wang J S, Wang J and Lü J T 2008 *Eur. Phys. J.* B **62** 381
[75] Peierls R 1929 *Ann. Phys.* **395** 1055
[76] Lindsay L, Broido D A and Mingo N 2009 *Phys. Rev.* B **80** 125407
[77] Lindsay L, Broido D A and Mingo N 2010 *Phys. Rev.* B **82** 115427
[78] Lindsay L, Broido D A and Mingo N 2011 *Phys. Rev.* B **83** 235428
[79] Maradudin A A and Vosko S H 1968 *Rev. Mod. Phys.* **40** 1
[80] Turney J E, Landry E S, McGaughey A J H and Amon C H 2009 *Phys. Rev.* B **79** 064301
[81] Xie G and Shen Y 2015 *Phys. Chem. Chem. Phys.* **17** 8822
[82] Shen Y L, Xie G F, Wei X L, Zhang K W, Tang M H, Zhong J X, Zhang G and Zhang Y W 2014 *J. Appl. Phys.* **115** 063507
[83] Nika D L and Balandin A A 2012 *J. Phys.: Condens. Matter* **24** 233203
[84] Schelling P K, Phillpot S R and Keblinski P 2002 *Phys. Rev.* B **65** 144306
[85] Sellan D P, Landry E S, Turney J E, McGaughey A J H and Amon C H 2010 *Phys. Rev.* B **81** 214305
[86] Ye Z, Cao B and Guo Z 2014 *Carbon* **66** 567
[87] Pereira L F C, Savić I and Donadio D 2013 *New J. Phys.* **15** 105019
[88] Cao A and Qu J 2012 *J. Appl. Phys.* **112** 013503
[89] Feng T, Ruan X, Ye Z and Cao B 2015 *Phys. Rev.* B **91** 224301
[90] Li X, Chen J, Yu C and Zhang G 2013 *Appl. Phys. Lett.* **103** 013111
[91] Hu M, Zhang X and Poulikakos D 2013 *Phys. Rev.* B **87** 195417
[92] Kim J Y, Lee J H and Grossman J C 2012 *ACS Nano* **6** 9050
[93] Zhang Y, Pei Q X, Wang C M, Yang C and Zhang Y W 2018 *J. Phys. Chem.* C **122** 22783
[94] Liu F, Zou R, Hu N, Ning H, Yan C, Liu Y, Wu L, Mo F and Fu S 2019 *Nanoscale* **11** 4067
[95] Chen J, Zhang G and Li B 2013 *Nanoscale* **5** 532
[96] Guo Z X, Ding J W and Gong X G 2012 *Phys. Rev.* B **85** 235429
[97] Turney J E, McGaughey A J H and Amon C H 2009 *Phys. Rev.* B **79** 224305
[98] Lü J T and Wang J S 2008 *J. Phys.: Condens. Matter* **21** 025503
[99] Wang J S 2007 *Phys. Rev. Lett.* **99** 160601
[100] Thomas J A, Turney J E, Iutzi R M, Amon C H and McGaughey A J H 2010 *Phys. Rev.* B **81** 081411
[101] Larkin J M, Turney J E, Massicotte A D, Amon C H and McGaughey A J H 2014 *J. Comput. Theor. Nanosci.* **11** 249
[102] Qiu B and Ruan X 2012 *Appl. Phys. Lett.* **100** 193101
[103] Qiu B, Bao H, Zhang G, Wu Y and Ruan X 2012 *Comput. Mater. Sci.* **53** 278
[104] Shi L, Li D, Yu C, Jang W, Kim D, Yao Z, Kim P and Majumdar A 2003 *J. Heat Transfer* **125** 881
[105] Wingert M C, Chen Z C Y, Kwon S, Xiang J and Chen R 2012 *Rev. Sci. Instrum.* **83** 024901
[106] Cahill D G, Katiyar M and Abelson J R 1994 *Phys. Rev.* B **50** 6077
[107] Choi T Y, Poulikakos D, Tharian J and Sennhauser U 2006 *Nano Lett.* **6** 1589
[108] Wang Z L, Tang D W, Li X B, Zheng X H, Zhang W G, Zheng L X, Zhu Y T, Jin A Z, Yang H F and Gu C Z 2007 *Appl. Phys. Lett.* **91** 123119
[109] Williams C C and Wickramasinghe H K 1986 *Appl. Phys. Lett.* **49** 1587
[110] Hsu I K, Kumar R, Bushmaker A, Cronin S B, Pettes M T, Shi L, Brintlinger T, Fuhrer M S and Cumings J 2008 *Appl. Phys. Lett.* **92** 063113
[111] Li Q, Liu C, Wang X and Fan S 2009 *Nanotechnology* **20** 145702
[112] Chen S, Wu Q, Mishra C, Kang J, Zhang H, Cho K, Cai W, Balandin A A and Ruoff R S 2012 *Nat. Mater.* **11** 203
[113] Yang L, Grassberger P and Hu B 2006 *Phys. Rev.* E **74** 062101
[114] Wang L, Hu B and Li B 2012 *Phys. Rev.* E **86** 040101
[115] Bae M H, Li Z, Aksamija Z, Martin P N, Xiong F, Ong Z Y, Knezevic I and Pop E 2013 *Nat. Commun.* **4** 1734
[116] Sahoo S, Gaur A P S, Ahmadi M, Guinel M J F and Katiyar R S 2013 *J. Phys. Chem.* C **117** 9042
[117] Jo I, Pettes M T, Lindsay L, Ou E, Weathers A, Moore A L, Yao Z and Shi L 2015 *AIP Adv.* **5** 053206
[118] Wang Y, Xu N, Li D and Zhu J 2017 *Adv. Funct. Mater.* **27** 1604134
[119] Cahill D G *et al* 2014 *Appl. Phys. Rev.* **1** 011305
[120] Chen B, Hoffmann R, Ashcroft N W, Badding J, Xu E and Crespi V 2015 *J. Am. Chem. Soc.* **137** 14373
[121] Xu E S, Lammert P E and Crespi V H 2015 *Nano Lett.* **15** 5124
[122] Zhan H, Zhang G, Bell J M and Gu Y 2016 *Carbon* **107** 304
[123] Wu W, Tai B, Guan S, Yang S A and Zhang G 2018 *J. Phys. Chem.* C **122** 3101
[124] Zhan H, Zhang G, Tan V B, Cheng Y, Bell J M, Zhang Y W and Gu Y 2016 *Adv. Funct. Mater.* **26** 5279
[125] Zhan H, Zhang G, Tan V B C and Gu Y 2017 *Nat. Commun.* **8** 14863
[126] Zhan H, Zhang G, Zhang Y, Tan V B C, Bell J M and Gu Y 2016 *Carbon* **98** 232
[127] Zhu T and Ertekin E 2016 *Nano Lett.* **16** 4763
[128] Xue Y, Chen Y, Li Z, Jiang J W, Zhang Y and Wei N 2019 *J. Phys. D: Appl. Phys.* **52** 085301
[129] Yamamoto T, Watanabe S and Watanabe K 2004 *Phys. Rev. Lett.* **92** 75502
[130] Mingo N and Broido D A 2005 *Nano Lett.* **5** 1221
[131] Kim P, Shi L, Majumdar A and McEuen P L 2001 *Phys. Rev. Lett.* **87** 215502

[132] Fujii M, Zhang X, Xie H, Ago H, Takahashi K, Ikuta T and Shimizu T 2005 *Phys. Rev. Lett.* **95** 065502
[133] Lukes J R and Zhong H 2007 *J. Heat Transfer* **129** 705
[134] Pop E, Mann D, Wang Q, Goodson K E and Dai H 2006 *Nano Lett.* **6** 96
[135] Yamamoto T, Konabe S, Shiomi J and Maruyama S 2009 *Appl. Phys. Express* **2** 095003
[136] Yan X H, Xiao Y and Li Z M 2006 *J. Appl. Phys.* **99** 124305
[137] Qiu B, Wang Y, Zhao Q and Ruan X 2012 *Appl. Phys. Lett.* **100** 233104
[138] Lindsay L, Broido D A and Mingo N 2010 *Phys. Rev.* B **82** 161402
[139] Yue S Y, Ouyang T and Hu M 2015 *Sci. Rep.* **5** 15440
[140] Ong Z Y, Pop E and Shiomi J 2011 *Phys. Rev.* B **84** 165418
[141] Zhong H and Lukes J R 2006 *Phys. Rev.* B **74** 125403
[142] Padgett C W and Brenner D W 2004 *Nano Lett.* **4** 1051
[143] Hu M, Jing Y and Zhang X 2015 *Phys. Rev.* B **91** 155408
[144] Ramazani A, Reihani A, Soleimani A, Larson R and Sundararaghavan V 2017 *Carbon* **123** 635
[145] Chen X K, Chen C Y, Liu J and Chen K Q 2017 *J. Phys. D: Appl. Phys.* **50** 345301
[146] Wang X M and Lu S S 2013 *J. Phys. Chem.* C **117** 19740
[147] Zhang J, Xu F, Hong Y, Xiong Q and Pan J 2015 *Rsc Adv.* **5** 89415
[148] Dollfus P, Nguyen V H and Saint-Martin J 2015 *J. Phys.: Condens. Matter* **27** 133204
[149] Liu C, Chen M, Yu W and He Y L 2018 *ES Energy Environ.* **2** 31
[150] Jauregui L A *et al* 2010 *ECS Trans.* **28** 73
[151] Zhang G 2017 *Thermal Transport in Carbon-Based Nanomaterials* (Amsterdam: Elsevier)
[152] Mingo N, Esfarjani K, Broido D A and Stewart D A 2010 *Phys. Rev.* B **81** 045408
[153] Polanco C A and Lindsay L 2018 *Phys. Rev.* B **97** 014303
[154] Cao B Y, Yao W J and Ye Z Q 2016 *Carbon* **96** 711
[155] Ong Z Y and Pop E 2011 *Phys. Rev.* B **84** 075471
[156] Wang Z, Xie R, Bui C T, Liu D, Ni X, Li B and Thong J T 2010 *Nano Lett.* **11** 113
[157] Prasher R S, Hu X J, Chalopin Y, Mingo N, Lofgreen K, Volz S, Cleri F and Keblinski P 2009 *Phys. Rev. Lett.* **102** 105901
[158] Rajabpour A, Fan Z and Vaez Allaei S M 2018 *Appl. Phys. Lett.* **112** 233104
[159] Yuan P, Zhang P, Liang T, Zhai S and Yang D 2019 *J. Mater. Sci.* **54** 1488
[160] Lindsay L and Kuang Y 2017 *Phys. Rev.* B **95** 121404
[161] Bonini N, Garg J and Marzari N 2012 *Nano Lett.* **12** 2673
[162] Lindsay L, Li W, Carrete J, Mingo N, Broido D A and Reinecke T L 2017 *Phys. Rev.* B **89** 155426
[163] Kuang Y, Lindsay L and Huang B 2015 *Nano Lett.* **15** 6121
[164] Lee S, Broido D, Esfarjani K and Chen G 2015 *Nat. Commun.* **6** 6290
[165] Cepellotti A, Fugallo G, Paulatto L, Lazzeri M, Mauri F and Marzari N 2015 *Nat. Commun.* **6** 6400
[166] Lee S and Lindsay L 2017 *Phys. Rev.* B **95** 184304
[167] Ding Z, Zhou J, Song B, Chiloyan V, Li M, Liu T H and Chen G 2018 *Nano Lett.* **18** 638
[168] Huberman S, Duncan R A, Chen K, Song B, Chiloyan V, Ding Z, Maznev A A, Chen G and Nelson K A 2019 *Science* **364** 375
[169] Xie Z X, Chen K Q and Duan W 2011 *J. Phys.: Condens. Matter* **23** 315302
[170] Morooka M, Yamamoto T and Watanabe K 2008 *Phys. Rev.* B **77** 033412
[171] Huang H, Xu Y, Zou X, Wu J and Duan W 2013 *Phys. Rev.* B **87** 205415
[172] Lahiri J, Lin Y, Bozkurt P, Oleynik I I and Batzill M 2010 *Nat. Nanotechnol.* **5** 326
[173] Li H, Ying H, Chen X, Nika D L, Cocemasov A I, Cai W, Balandin A A and Chen S 2014 *Nanoscale* **6** 13402
[174] Malekpour H, Ramnani P, Srinivasan S, Balasubramanian G, Nika D L, Mulchandani A, Lake R K and Balandin A A 2016 *Nanoscale* **8** 14608
[175] Wei N, Xu L, Wang H Q and Zheng J C 2011 *Nanotechnology* **22** 105705
[176] Guo Z, Zhang D and Gong X G 2009 *Appl. Phys. Lett.* **95** 163103
[177] Gunawardana K G.S H, Mullen K, Hu J, Chen Y P and Ruan X 2012 *Phys. Rev.* B **85** 245417
[178] Yeo P S E, Loh K P and Gan C K 2012 *Nanotechnology* **23** 495702
[179] Chen X K, Xie Z X, Zhou W X and Chen K Q 2016 *J. Phys. D: Appl. Phys.* **49** 115301
[180] Zhu T and Ertekin E 2015 *Phys. Rev.* B **91** 205429
[181] Wang C, Liu Y, Li L and Tan H 2014 *Nanocale* **6** 5703
[182] Pei Q X, Sha Z D and Zhang Y W 2011 *Carbon* **49** 4752
[183] Barbarino G, Melis C and Colombo L 2014 *Carbon* **80** 167
[184] Mu X, Wu X, Zhang T, Go D B and Luo T 2014 *Sci. Rep.* **4** 3909
[185] Chien S K and Yang Y T 2012 *Carbon* **50** 421
[186] Xie G, Ding D and Zhang G 2018 *Adv. Phys.* X **3** 719
[187] Maldovan M 2015 *Nat. Mater.* **14** 667
[188] Xie G, Ju Z, Zhou K, Wei X, Guo Z, Cai Y and Zhang G 2018 *NPJ Comput. Mater.* **4** 21
[189] Luckyanova M N *et al* 2012 *Science* **338** 936
[190] Ravichandran J *et al* 2014 *Nat. Mater.* **13** 168
[191] Mu X, Zhang T, Go D B and Luo T 2015 *Carbon* **83** 208
[192] Shiomi J and Maruyama S 2006 *Phys. Rev.* B **74** 155401
[193] Ouyang T, Chen Y P, Yang K K and Zhong J 2009 *Europhys. Lett.* **88** 28002
[194] Yang L, Chen J, Yang N and Li B 2015 *Int. J. Heat Mass Transfer* **91** 428
[195] Davis B L and Hussein M I 2014 *Phys. Rev. Lett.* **112** 055505
[196] Xiong S, Saaskilahti K, Kosevich Y A, Han H, Donadio D and Volz S 2016 *Phys. Rev. Lett.* **117** 025503
[197] Giri A and Hopkins P E 2018 *Phys. Rev.* B **98** 045421
[198] Ma D, Wan X and Yang N 2018 *Phys. Rev.* B **98** 245420
[199] Chen X K, Liu J, Xie Z X, Zhang Y, Deng Y X and Chen K Q 2018 *Appl. Phys. Lett.* **113** 121906
[200] Li G, Li Y, Liu H, Guo Y, Li Y and Zhu D 2010 *Chem. Commun.* **46** 3256
[201] Ouyang T, Chen Y, Liu L M, Xie Y, Wei X and Zhong J 2012 *Phys. Rev.* B **85** 235436
[202] Chen X K, Liu J, Du D and Chen K Q 2017 *J. Phys.: Condens. Matter* **29** 455702
[203] Zhang Y Y, Pei Q X and Wang C M 2012 *Comput. Mater. Sci.* **65** 406
[204] Wang S W, Si Y, Yuan J, Yang B and Chen H 2016 *Phys. Chem. Chem. Phys.* **18** 24210
[205] Gao Y, Zhang X, Tang D and Hu M 2019 *Carbon* **143** 189
[206] Zhou W X and Chen K Q 2015 *Carbon* **85** 24
[207] Zhang Y Y, Pei Q X, Hu M and Zong Z 2015 *RSC Adv.* **5** 65221
[208] Xia K L, Artyukhov V I, Sun L F, Zheng J Y, Jiao L Y, Yakobson B I and Zhang Y Y 2016 *Nano Res.* **9** 2182
[209] Cranford S W 2016 *Carbon* **96** 421
[210] Wang F Q, Yu J, Wang Q, Kawazoe Y and Jena P 2016 *Carbon* **105** 424
[211] Wang F Q, Liu J, Li X, Wang Q and Kawazoe Y 2017 *Appl. Phys. Lett.* **111** 192102
[212] Zou J H, Ye Z Q and Cao B Y 2016 *J. Chem. Phys.* **145** 134705
[213] Winczewski S, Shaheen M Y and Rybicki J 2018 *Carbon* **126** 165
[214] Erhart P and Albe K 2005 *Phys. Rev.* B **71** 035211
[215] Xu W, Zhang G and Li B 2015 *J. Chem. Phys.* **143** 154703
[216] Wu X, Varshney V, Lee J, Zhang T, Wohlwend J L, Roy A K and Luo T 2016 *Nano Lett.* **16** 3925

[217] Zhang Y Y, Pei Q X, Cheng Y, Zhang Y W and Zhang X 2017 *Comput. Mater. Sci.* **137** 195
[218] Weng H, Liang Y, Xu Q, Yu R, Fang Z, Dai X and Kawazoe Y 2015 *Phys. Rev.* B **92** 045148
[219] Chen Y P, Xie Y, Yang S A, Pan H, Zhang F, Cohen M L and Zhang S 2015 *Nano Lett.* **15** 6974
[220] Chen S Z, Zhou W X, Yu J F and Chen K Q 2018 *Carbon* **129** 809
[221] Varshney V, Patnaik S S, Roy A K, Froudakis G and Farmer B L 2010 *ACS Nano* **4** 1153
[222] Xu L, Wei N, Zheng Y, Fan Z, Wang H Q and Zheng J C 2012 *J. Mater. Chem.* **22** 1435
[223] Chen J *et al* 2012 *ACS Appl. Mater. Interfaces* **4** 81
[224] Pang Z, Gu X, Wei Y, Yang R and Dresselhaus M S 2016 *Nano Lett.* **17** 179
[225] Chen S Z, Deng Y X, Cao X H, Zhou W X, Feng Y X, Tang L M and Chen K Q 2019 *J. Mater. Chem.* A **7** 21976
[226] Chen S Z, Xie F, Ning F, Liu Y Y, Zhou W X, Yu J F and Chen K Q 2017 *Carbon* **111** 867
[227] Wei Z, Yang F, Bi K, Yang J and Chen Y 2017 *Carbon* **113** 212
[228] Chen X K, Liu J, Du D, Xie Z X and Chen K Q 2018 *J. Phys.: Condens. Matter* **30** 155702
[229] Gu X, Pang Z, Wei Y and Yang R 2017 *Carbon* **119** 278
[230] Han Y, Yang J Y and Hu M 2018 *Nanoscale* **10** 5229
[231] Zhang J 2018 *Carbon* **131** 127
[232] Yang D J, Zhang Q, Chen G, Yoon S F, Ahn J, Wang S G, Zhou Q, Wang Q and Li J Q 2002 *Phys. Rev.* B **66** 165440
[233] Wang X, Zhong Z and Xu J 2005 *J. Appl. Phys.* **97** 064302
[234] Son Y, Pal S K, Borca-Tasciuc T, Ajayan P M and Siegel R W 2008 *J. Appl. Phys.* **103** 024911
[235] Hamdan A, Cho J, Johnson R, Jiao J, Bahr D, Richards R and Richards C 2010 *Nanotechnology* **21** 015702
[236] Panzer M A, Zhang G, Mann D, Hu X, Pop E, Dai H and Goodson K E 2008 *J. Heat Transfer* **130** 052401
[237] Feng Y, Zhu J and Tang D 2018 *Appl. Therm. Eng.* **145** 667
[238] Cola B A, Xu X and Fisher T S 2007 *Appl. Phys. Lett.* **90** 093513
[239] Ong Z Y and Pop E 2010 *Phys. Rev.* B **81** 155408
[240] Kaur S, Raravikar N, Helms B A, Prasher R and Ogletree D F 2014 *Nat. Commun.* **5** 3082
[241] Gao Y *et al* 2013 *Nano Lett.* **13** 3439
[242] Sun J, Zheng G, Lee H W, Liu N, Wang H, Yao H, Yang W and Cui Y 2014 *Nano Lett.* **14** 4573
[243] Song J and Medhekar N V 2013 *J. Phys.: Condens. Matter* **25** 445007
[244] Ong Z Y, Zhang G and Zhang Y W 2016 *Phys. Rev.* B **93** 075406
[245] Feng T, Yao W, Wang Z, Shi J, Li C, Cao B and Ruan X 2017 *Phys. Rev.* B **95** 195202
[246] Lu J, Gomes L C, Nunes R C, Castro Neto A H and Loh K P 2014 *Nano Lett.* **14** 5133
[247] Liu X, Zhang G and Zhang Y W 2016 *Nano Lett.* **16** 4954
[248] Li M, Zhang B, Duan K, Zhang Y, Huang Z and Zhou H 2018 *J. Phys. Chem.* C **122** 14945
[249] Liu X, Gao J, Zhang G and Zhang Y W 2017 *Nano Res.* **10** 2944
[250] Liu X, Gao J, Zhang G and Zhang Y W 2018 *Nanoscale* **10** 19854
[251] Liu B, Baimova J A, Reddy C D, Dmitriev S V, Law W K, Feng X Q and Zhou K 2014 *Carbon* **79** 236
[252] Yokomizo Y and Nakamura J 2013 *Appl. Phys. Lett.* **103** 113901
[253] Li S, Ren Z, Zheng J, Zhou Y, Wan Y and Hao L 2013 *J. Appl. Phys.* **113** 033703
[254] Zhu T and Eretkin E 2014 *Phys. Rev.* B **90** 195209
[255] Silva C D, Saiz F, Romero D A and Amon C H 2016 *Phys. Rev.* B **93** 125427
[256] Chen X K, Xie Z X, Zhou W X, Tang L M and Chen K Q 2016 *Appl. Phys. Lett.* **109** 023101
[257] Wang X, Wang M, Hong Y, Wang Z and Zhang J 2017 *Phys. Chem. Chem. Phys.* **19** 24240
[258] Le N B, Huan T D and Woods L M 2016 *ACS Appl. Mater. Interfaces* **8** 6286
[259] Argentero G, Mittelberger A, Monazam M R A, Cao Y, Pennycook T J, Mangler C, Kramberger C, Kotakoski J, Geim A K and Meyer J C 2017 *Nano Lett.* **17** 1409
[260] Jung S, Park M, Park J, Jeong T Y, Kim H J, Watanabe K, Taniguchi T, Dong H H, Hwang C and Kim Y S 2015 *Sci. Rep.* **5** 16642
[261] Zhang Z, Hu S, Chen J and Li B 2017 *Nanotechnology* **28** 225704
[262] Pak A J and Hwang G S 2016 *Phys. Rev. Appl.* **6** 034015
[263] Zou J H and Cao B Y 2017 *Appl. Phys. Lett.* **110** 103106
[264] Yan Z, Chen L, Yoon M and Kumar S 2016 *Nanoscale* **8** 4037
[265] Chen C C, Li Z, Shi L and Cronin S B 2014 *Appl. Phys. Lett.* **104** 081908
[266] Hong Y, Zhang J and Zeng X C 2016 *Nanoscale* **8** 19211
[267] Hong Y, Zhu C, Ju M, Zhang J and Zeng X C 2017 *Phys. Chem. Chem. Phys.* **19** 6554
[268] Hong Y, Ju M G, Zhang J and Zeng X C 2018 *Phys. Chem. Chem. Phys.* **20** 2637
[269] Liu B, Meng F, Reddy C D, Baimova J A, Srikanth N, Dmitriev S V and Zhou K 2015 *RSC Adv.* **5** 29193
[270] Liu B, Baimova J A, Reddy C D, Law A W K, Dmitriev S V, Wu H and Zhou K 2014 *ACS Appl. Mater. Interfaces* **6** 18180
[271] Chae H G and Kumar S 2008 *Science* **319** 908
[272] Shen S, Henry A, Tong J, Zheng R and Chen G 2010 *Nat. Nanotechnol.* **5** 251
[273] Liu J and Yang R 2010 *Phys. Rev.* B **81** 174122
[274] Bonnet P, Sireude D, Garnier B and Chauvet O 2007 *Appl. Phys. Lett.* **91** 201910
[275] Han Z and Fina A 2011 *Prog. Polym. Sci.* **36** 914
[276] Haggenmueller R, Guthy C, Lukes J R, Fischer J E and Winey K I 2007 *Macromolecules* **40** 2417
[277] Zhang X *et al* 2011 *Nano Lett.* **11** 3239
[278] Marconnet A M, Yamamoto N, Panzer M A, Wardle B L and Goodson K E 2011 *ACS Nano* **5** 4818
[279] Yu C, Choi K, Yin L and Grunlan J C 2011 *ACS Nano* **5** 7885
[280] Fan L W, Fang X, Wang X, Zeng Y, Xiao Y Q, Yu Z T, Xu X, Hu Y C and Cen K F 2013 *Appl. Energy* **110** 163
[281] Martin-Gallego M, Verdejo R, Khayet M, de Zarate J M O, Essalhi M and Lopez-Manchado M A 2011 *Nanoscale Res. Lett.* **6** 610
[282] Yu A, Ramesh P, Sun X, Bekyarova E, Itkis M E and Haddon R C 2008 *Adv. Mater.* **20** 4740
[283] Shtein M, Nadiv R, Buzaglo M and Regev O 2015 *ACS Appl. Mater. Interfaces* **7** 23725
[284] Teng C C, Ma C C M, Lu C H, Yang S Y, Lee S H, Hsiao M C, Yen M Y, Chiou K C and Lee T M 2011 *Carbon* **49** 5107
[285] Li X, Fan X, Zhu Y, Li J, Adams J M, Shen S and Li H 2012 *Comput. Mater. Sci.* **63** 207
[286] Eslami H and Behrouz M 2014 *J. Phys. Chem.* C **118** 9841
[287] Huang H, Chen L, Varshney V, Roy A K and Kumar S 2016 *J. Appl. Phys.* **120** 095102
[288] Ni Y, Han H, Volz S and Dumitrică T 2015 *J. Phys. Chem.* C **119** 12193
[289] Wang Y, Yang C, Mai Y W and Zhang Y 2016 *Carbon* **102** 311
[290] Lin S and Buehler M J 2013 *Nanotechnology* **24** 165702
[291] Shen X, Wang Z, Wu Y, Liu X and Kim J K 2016 *Carbon* **108** 412

[292] Cao B Y, Zou J H, Hu G J and Cao G X 2018 *Appl. Phys. Lett.* **112** 041603
[293] Gao Y and Müller-Plathe F 2016 *J. Phys. Chem.* B **120** 1336
[294] Li M, Zhou H, Zhang Y, Liao Y and Zhou H 2018 *Carbon* **130** 295
[295] Xie R, Bui C T, Varghese B, Zhang Q, Sow C H, Li B and Thong J T L 2011 *Adv. Funct. Mater.* **21** 1602
[296] Ni X, Zhang G and Li B 2011 *J. Phys.: Condens. Matter* **23** 215301
[297] Yang N, Zhang G and Li B 2009 *Appl. Phys. Lett.* **95** 033107
[298] Liu Y Y, Zhou W X, Tang L M and Chen K Q 2014 *Appl. Phys. Lett.* **105** 203111
[299] Xie Z, Li K M, Tang L M, Pan C N and Chen K Q 2012 *Appl. Phys. Lett.* **100** 183110
[300] Wang Y, Vallabhaneni A, Hu J, Qiu B, Chen Y P and Ruan X 2014 *Nano Lett.* **14** 592
[301] Wang Y, Chen S and Ruan X 2012 *Appl. Phys. Lett.* **100** 163101
[302] Wang H, Hu S, Takahashi K, Zhang X, Takamatsu H and Chen J 2017 *Nat. Commun.* **8** 15843
[303] Gordiz K and Mehdi Vaez Allaei S 2014 *J. Appl. Phys.* **115** 163512
[304] Yuan K, Sun M, Wang Z and Tang D 2015 *Int. J. Therm. Sci.* **98** 24
[305] Pal S and Puri I K 2014 *Nanotechnology* **25** 345401
[306] Melis C, Barbarino G and Colombo L 2015 *Phys. Rev.* B **92** 245408
[307] Chen X K, Xie Z X, Zhang Y, Deng Y X, Zou T H and Chen K Q 2019 *Carbon* **148** 532
[308] Chen X K, Xie Z X, Zhou W X, Tang L M and Chen K Q 2016 *Carbon* **100** 492
[309] Chen X K, Ju J W, Wu X J, Jia P, Peng Z H and Chen K Q 2018 *J. Phys. D: Appl. Phys.* **51** 085103
[310] Sandonas L M, Cuba-Supanta G, Gutierrez R, Dianat A, Landauro C V and Cuniberti G 2018 *Carbon* **124** 642
[311] Yang X, Yu D, Cao B and To A C 2017 *ACS Appl. Mater. Interfaces* **9** 24078
[312] Yang X, Xu J, Wu S, Yu D and Cao B 2018 *J. Phys.: Condens. Matter* **30** 435305
[313] Zhang T and Luo T 2015 *Small* **11** 4657
[314] Cottrill A L and Strano M S 2015 *Adv. Energy Mater.* **5** 1500921
[315] Chen X K, Liu J, Peng Z H, Du D and Chen K Q 2017 *Appl. Phys. Lett.* **110** 091907
[316] Ai B Q, An M and Zhong W R 2013 *J. Chem. Phys.* **138** 034708
[317] Pal S and Puri I K 2015 *Small* **11** 2910
[318] Zhong W R, Zhong D Q and Hu B 2012 *Nanoscale* **4** 5217
[319] Hicks L D and Dresselhaus M S 1993 *Phys. Rev.* B **47** 12727
[320] Xie Z X, Tang L M, Pan C N, Li K M, Chen K Q and Duan W 2012 *Appl. Phys. Lett.* **100** 073105
[321] Mazzamuto F, Nguyen V H, Apertet Y, Caër C, Chassat C, Saint-Martin J and Dollfus P 2011 *Phys. Rev.* B **83** 235426
[322] Huang W, Wang J S and Liang G 2011 *Phys. Rev.* B **84** 045410
[323] Tran V T, Saint-Martin J and Dollfus P 2015 *Nanotechnology* **26** 495202
[324] Sevinçli H, Sevik C, Çağın T and Cuniberti G 2013 *Sci. Rep.* **3** 1228
[325] Tan S and Chen K Q 2015 *Carbon* **94** 942
[326] Hung Nguyen V, Nguyen M C, Nguyen H V, Saint-Martin J and Dollfus P 2014 *Appl. Phys. Lett.* **105** 133105
[327] Cui X, Ouyang T, Li J, He C, Tang C and Zhong J 2018 *Phys. Chem. Chem. Phys.* **20** 7173
[328] Fan Z Q, Chen K Q, Wang Q, Zou B S, Duan W and Shuai Z 2008 *Appl. Phys. Lett.* **92** 263304
[329] Ren Y, Chen K Q, He J, Tang L M, Pan A, Zou B S and Zhang Y 2010 *Appl. Phys. Lett.* **97** 103506
[330] Chen T, Li H, Zhang Y, Liu D, Chao Y and Wang L 2017 *J. Electron. Mater.* **46** 5121
[331] Chen T, Xu L, Li Q, Li X and Long M 2019 *Nanotechnology* **30** 445703
[332] Xu L, Huang W Q, Hu W, Yang K, Zhou B X, Pan A and Huang G F 2017 *Chem. Mater.* **29** 5504
[333] Peng X F, Chen K Q, Wan Q, Zou B S and Duan W 2010 *Phys. Rev.* B **81** 195317
[334] Chen K Q, Wang X H and Gu B Y 2000 *Phys. Rev.* B **61** 12075
[335] Liu Y Y, Zeng Y J, Jia P Z, Cao X H, Jiang X and Chen K Q 2018 *J. Phys.: Condens. Matter* **30** 275701
[336] Xie Z X, Zhang Y, Zhang L F and Fan D Y 2017 *Carbon* **113** 292
[337] Bürkle M, Hellmuth T J, Pauly F and Asai Y 2015 *Phys. Rev.* B **91** 165419
[338] Cao X H, Zhou W X, Chen C Y, Tang L M, Long M and Chen K Q 2017 *Sci. Rep.* **7** 10842
[339] Cao X H, Wu D, Feng Y X, Zhou W X, Tang L M and Chen K Q 2019 *J. Phys.: Condens. Matter* **31** 345303
[340] Perroni C A, Ninno D and Cataudella V 2016 *J. Phys.: Condens. Matter* **28** 373001
[341] Zeng Y J, Wu D, Cao X H, Zhou W X, Tang L M and Chen K Q 2019 *Adv. Funct. Mater.* (https://doi.org/10.1002/adfm.201903873)
[342] Wu D, Cao X H, Chen S Z, Tang L M, Feng Y X, Chen K Q and Zhou W X 2019 *J. Mater. Chem.* A **7** 19037
[343] Li B L and Chen K Q 2016 *J. Phys.: Condens. Matter* **29** 075301
[344] Liu Y Y, Li B L, Chen S Z, Jiang X and Chen K Q 2017 *Appl. Phys. Lett.* **111** 133107
[345] Li B L and Chen K Q 2017 *Carbon* **119** 548